Bacterial Biofilm Material Properties Enable Removal and Transfer by Capillary Peeling

Jing Yan, Alexis Moreau, Sepideh Khodaparast, Antonio Perazzo, Jie Feng, Chenyi Fei, Sheng Mao, Sampriti Mukherjee, Andrej Košmrlj, Ned S. Wingreen, Bonnie L. Bassler,* and Howard A. Stone*

Biofilms, surface-attached communities of bacterial cells, are a concern in health and in industrial operations because of persistent infections, clogging of flows, and surface fouling. Extracellular matrices provide mechanical protection to biofilm-dwelling cells as well as protection from chemical insults, including antibiotics. Understanding how biofilm material properties arise from constituent matrix components and how these properties change in different environments is crucial for designing biofilm removal strategies. Here, using rheological characterization and surface analyses of *Vibrio cholerae* biofilms, it is discovered how extracellular polysaccharides, proteins, and cells function together to define biofilm mechanical and interfacial properties. Using insight gained from our measurements, a facile capillary peeling technology is developed to remove biofilms from surfaces or to transfer intact biofilms from one surface to another. It is shown that the findings are applicable to other biofilm-forming bacterial species and to multiple surfaces. Thus, the technology and the understanding that have been developed could potentially be employed to characterize and/or treat biofilm-related infections and industrial biofouling problems.

Biofilms are surface-attached communities of bacteria that cause problems including medical infections, fouling, and clogging in industrial applications.[1] By contrast, beneficial biofilms are crucial in applications including waste-water treatment and microbial fuel cells.[2] To solve biofilm-related problems and to realize the potential of biofilm-promoting technologies,

Dr. J. Yan, A. Moreau, Dr. S. Khodaparast, Dr. A. Perazzo, Dr. J. Feng,
Dr. S. Mao, Prof. A. Košmrlj, Prof. H. A. Stone
Department of Mechanical and Aerospace Engineering
Princeton University
D328 E-Quad, Olden St., Princeton, NJ 08544, USA
E-mail: hastone@princeton.edu
C. Fei, Dr. S. Mukherjee, Prof. N. S. Wingreen, Prof. B. L. Bassler
Department of Molecular Biology
Princeton University
329 Lewis Thomas Laboratory, Princeton, NJ 08544, USA
E-mail: bbassler@princeton.edu
Prof. B. L. Bassler
Howard Hughes Medical Institute
Chevy Chase, MD 20815, USA

The ORCID identification number(s) for the author(s) of this article can be found under https://doi.org/10.1002/adma.201804153.

understanding of both the biological and physical properties of biofilms and how these properties interrelate[3] is necessary. Compared to the extensively studied biological components and regulatory networks responsible for biofilm formation,[4] how the material properties of biofilms are derived from the constituent biocomponents and how biofilm mechanics change in response to environmental fluctuations are not understood.[5] Similar to synthetic hydrogels, biofilms are composed primarily of water (90%), yet they possess structural integrity and they protect biofilm-dwelling cells from external perturbations such as biocides, shear flows, phagocytosis, and invasion by other bacterial species.[5a,6] Biofilm matrices are composed of extracellular polysaccharides, accessory proteins, and in some cases, extracellular DNA. Recently, mechanical properties of biofilms have been measured using rheological tools.[5c,7] However, physical interpretation of biofilm rheological data is not straightforward due to the structural complexity of biofilms,[8] impeding the establishment of general mechanical principles for understanding, disrupting, or, more forward-looking, designing biofilm materials.[9]

The majority of investigations of biofilm material characteristics have focused on bulk biofilm properties, not on their surfaces. However, biofilm interfacial properties are crucial in driving their overall material responses,[10] particularly with respect to how biofilms will interact with underlying substrates. Understanding biofilm interfacial properties could lead to insights relevant to biofilm-related problems. For example, in the context of biofilm removal via mechanical disruption, which is often the first strategy for treating biofilm infections in wounds and in some industrial applications,[5c,11] to avoid leaving residual biofilm patches, it could be more desirable to detach entire biofilms from the substrate rather than to disrupt biofilms at the wound site or at the contaminated surface. In the language of mechanics, in some cases, inducing interfacial fracture between a biofilm and the substrate could be superior to inducing cohesive fracture within a biofilm. However, to successfully induce interfacial fracture, a deeper understanding of biofilm surface properties is needed.
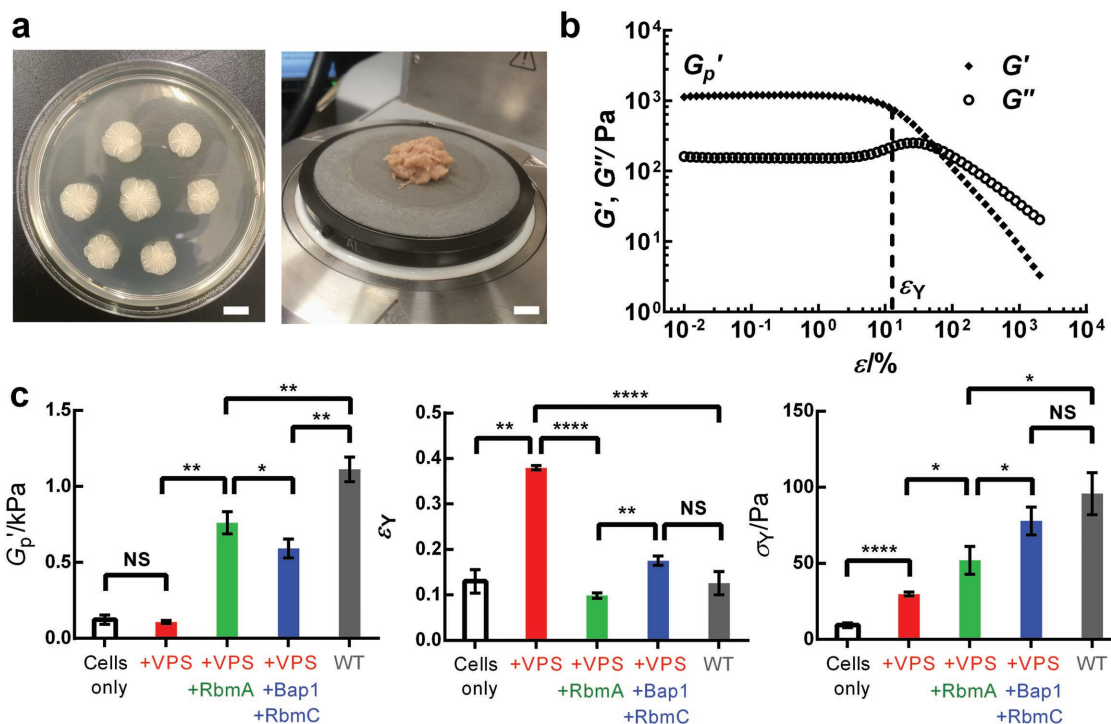
Figure 1. Rheological characterization of *V. cholerae* biofilms. a) Representative images of WT biofilms grown for two days on LB medium solidified with 0.6% agar (left) and following transfer to the lower plate of a rheometer (right). Scale bars: 1 cm. b) Representative storage modulus G' and loss modulus G'' curves as a function of the amplitude of oscillatory shear strain ε measured for the biofilm sample in (a). From the G' curves, plateau storage modulus G'_p and yield strain ε_Y (indicated by the vertical dotted line) were extracted for each biofilm. c) Measured G'_p, ε_Y, and yield stress σ_Y values, from left to right, for biofilms containing cells only ($\Delta rbmA \Delta bap1 \Delta rbmC \Delta vpsL$, white), cells and the vibrio polysaccharide (VPS) ($\Delta rbmA \Delta bap1 \Delta rbmC$, red), and with RbmA ($\Delta bap1 \Delta rbmC$, green), and with RbmC and Bap1 ($\Delta rbmA$, blue), and with all the matrix components (WT, gray), respectively. All biofilms were grown for two days on LB medium solidified with 0.6% agar. Unpaired *t*-tests with Welch's correction were performed for statistical analyses. NS denotes not significant; * denotes $P < 0.05$, ** denotes $P < 0.01$, **** denotes $P < 0.0001$. Error bars correspond to standard deviations with $n = 3$.

Here, we use the model biofilm forming bacterium *Vibrio cholerae*, the causative agent of the pandemic disease cholera,[12] to investigate how biofilm material properties are determined by their components. Our measurements reveal *V. cholerae* biofilms to be soft viscoelastic solids similar to hydrogels, with surface polarity/hydrophobicity that depends on particular matrix components. We develop a capillary peeling method as a practical and efficient technique to remove biofilms from various surfaces via interfacial fracture. The capillary peeling technique also provides a means to measure the adhesion energy between biofilms and substrates, and, moreover, enables the easy transfer of intact biofilms from one surface to another without destroying their internal structures.

To examine biofilm mechanics, we use a commonly studied immotile *V. cholerae* mutant that constitutively forms biofilms.[13] This strain is denoted wild type (WT). We grew *V. cholerae* biofilms on a soft nutritious substrate (LB medium solidified with different concentrations of agar, **Figure 1**a). To measure biofilm mechanical properties, we transferred the biofilm biomass to a shear rheometer (Figure 1a).[14] Oscillatory shear stresses were applied, and by measuring the resulting strains, we deduced the storage modulus G' (representative of the elastic, solid-like properties) and the loss modulus G'' (representative of the viscous, fluid-like properties) of the biofilm as a function of the amplitude of the oscillatory strain

ε.[15] Figure 1b shows that biofilms are viscoelastic solids, similar to hydrogels[15,16]: the biofilm possesses a shear modulus G' that is ≈10 times larger than G''. Indeed, the measured G' value is close to the value previously derived using classical hydrogel theory.[13b] The $G'(\varepsilon)$ curve features an initial plateau region in which the biofilm deforms elastically with increasing external stresses, which allows the definition of the plateau modulus of a biofilm, G'_p. Above a critical strain, referred to as the yield strain ε_Y, the biofilm starts to yield with a dramatic decrease in G'. Concomitantly, G'' displays a peak signifying an increase in energy dissipation during the yielding process. All of these mechanical behaviors are analogous to those of hydrogels.[7a,15,16] Consistent with this analogy, both G' and G'' of a biofilm show only slight frequency dependence in the linear viscoelastic regime (Figure S1, Supporting Information).

To define the structural elements responsible for biofilm mechanics, we generated *V. cholerae* mutants lacking particular matrix components.[17] In *V. cholerae*, the vibrio polysaccharide (VPS), a hydrophilic polymer composed primarily of glucose and galactose and other minor building blocks,[18] serves as the main scaffold for the extracellular matrix.[19] The accessory protein RbmA connects neighboring cells by dimerizing and interacting with VPS through extensive surface binding.[20] Two other proteins with high homology, Bap1 and RbmC, perform partially redundant functions in which Bap1 more than
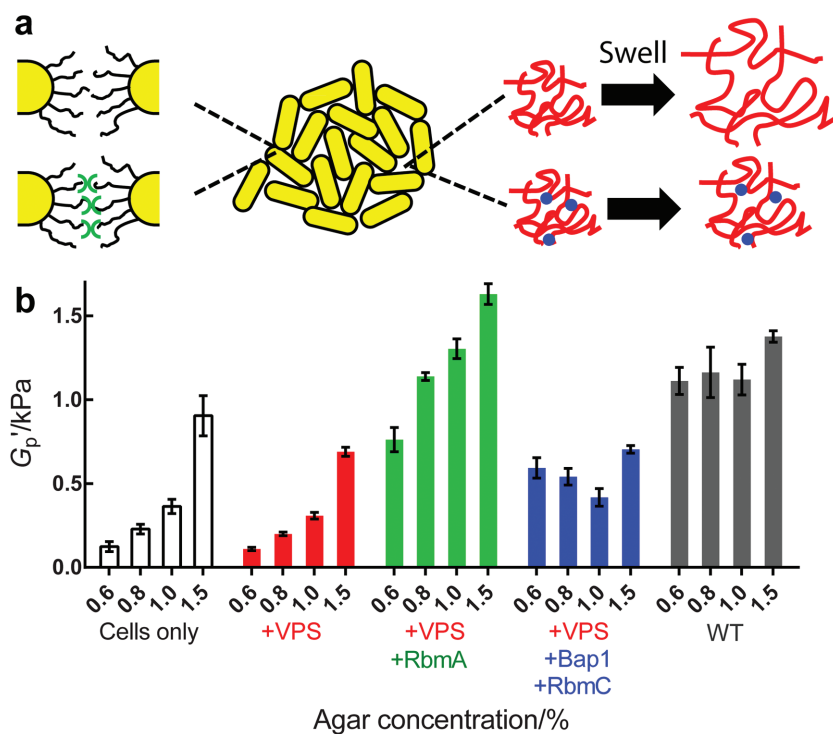
**ADVANCED
SCIENCE NEWS**

www.advancedsciencenews.com

**ADVANCED
MATERIALS**

www.advmat.de

Figure 2. Osmotic pressure affects the biofilm plateau modulus and the effect depends on particular matrix components. a) Schematic of the *V. cholerae* biofilm matrix components contributing to its mechanical properties. The yellow cylinders denote cells. The black curvy lines (left) denote cell surface LPS. The red wavy lines (right) denote VPS filling interstitial spaces. The blue dots (right bottom) denote the RbmC and Bap1 proteins that crosslink the VPS network. The green symbols (bottom left) denote RbmA proteins that connect neighboring cells. b) Shown from left to right are the plateau storage moduli G'_p for biofilms containing cells only ($\Delta rbmA\Delta bap1\Delta rbmC\Delta vpsL$, white), cells and VPS ($\Delta rbmA\Delta bap1\Delta rbmC$, red), and with RbmA ($\Delta bap1\Delta rbmC$, green), and with RbmC and Bap1 ($\Delta rbmA$, blue), and with all matrix components (WT, gray), grown on medium solidified with the designated concentrations of agar, respectively. The error bars correspond to standard deviations with $n = 3$.

RbmC is responsible for cell-surface adhesion and RbmC more than Bap1 provides additional crosslinks with the VPS.[21] We generated single, double, triple, and quadruple mutants to systematically investigate the distinct contribution of each matrix component to biofilm mechanics.

We first present data for biofilms grown on the softest agar we tested (0.6%). Figure 1c shows the measured plateau modulus G'_p (left) and yield strain ε_Y (middle) for each bacterial strain. The quadruple mutant $\Delta rbmA\Delta bap1\Delta rbmC\Delta vpsL$ (white) exhibits a low basal G'_p ($\approx$120 Pa) and ε_Y ($\approx$0.1). Upon introduction of an unstructured extracellular matrix (i.e., +VPS), the $\Delta rbmA\Delta bap1\Delta rbmC$ (red) strain displays a similar G'_p to the quadruple mutant but possesses a significantly increased yield strain ε_Y ($\approx$0.4). When the cell–cell linkage protein RbmA is present ($\Delta bap1\Delta rbmC$ strain, green), the biofilm shows increased elasticity ($G'_p \approx 760$ Pa), although at a cost of reduced ε_Y ($\approx$0.1). Similarly, in the $\Delta rbmA$ strain (blue), the presence of RbmC/Bap1 causes G'_p to increase to $\approx$590 Pa. Finally, the WT strain (gray) exhibits the largest G'_p, around 1 kPa with a small ε_Y ($\approx$0.1). We also plotted the yield stress σ_Y (the product of G'_p and ε_Y), which indicates the maximum shear stress a biofilm can sustain before it begins to yield, for the WT and mutant biofilms

(Figure 1c, right). A monotonic increase in σ_Y occurred as components are incorporated into the biofilm matrix, from $\approx$10 Pa for the quadruple mutant biofilm to $\approx$100 Pa for the WT biofilm. In nature, *V. cholerae* biofilms grow on sinking marine particles or on swimming organisms and so they are subjected to flow-induced shear stress.[22] Our results suggest that the flow environment could impose a selective pressure on *V. cholerae* to evolve multiple matrix components that enable the biofilms to withstand shear stress.

We propose a dual network model to understand the mechanical properties of *V. cholerae* biofilms (**Figure 2**a). The key is the presence of two interacting networks, one composed of interconnected, stiff bacterial cells, and the other composed of soft secreted polymers.[23] In the quadruple mutant, cells are in direct contact with one another, and we propose that neighboring cells interact weakly through their surface lipopolysaccharides (LPS) or other surface appendages such as pili.[24] Similar to colloidal gels with short-range attractions,[25] this cellular network yields at a relatively low strain, $\varepsilon_Y \approx 0.1$. In the $\Delta rbmA\Delta bap1\Delta rbmC$ biofilm that lacks accessory proteins but possesses the VPS polysaccharides, VPS fills the spaces between neighboring cells and increases ε_Y to $\approx$0.4 (Figure 1c, red). Cells interact indirectly through the hydrogel network of the VPS, which can sustain larger deformations than the naked cells. However, our measurements show that the unstructured VPS does not increase the biofilm storage modulus, presumably because the hydrogen-bond-based interactions between individual polysaccharide chains are similar to those between individual LPS units.[26] To strengthen the biofilm, two strategies are employed. First, the polymer network is reinforced by cross-linking via RbmC/Bap1 (Figure 1c, blue).[21a,27] Second, the cellular network is strengthened by enhancing the weak cell–cell interactions via crosslinking by RbmA.[20,28] In the latter case, a stronger colloidal gel with short-range attractions forms,[25] and hence ε_Y once again declines while G'_p increases (Figure 1c, green). Note that the strengthening effect of RbmA depends on VPS and RbmC/Bap1 (Figure S2, Supporting Information), suggesting that the two networks function together to fortify the *V. cholerae* biofilm. Indeed, the WT biofilm possesses both the cell–cell and polymeric networks so it exhibits the highest G'_p ($\approx$1 kPa), despite a small ε_Y due to the short-range nature of RbmA-mediated cell–cell interactions. Future experiments investigating the rheology of combinations of purified matrix components will be necessary to provide a molecular-level understanding of how the precise interactions between particular matrix components and between matrix components and cells drive macroscopic biofilm mechanics.

Biofilm mechanical properties often depend on physicochemical conditions.[7c,14,29] This feature has often been

**ADVANCED
SCIENCE NEWS**
www.advancedsciencenews.com

**ADVANCED
MATERIALS**
www.advmat.de

attributed to biological responses to the environment, directed by gene expression changes. However, we hypothesized that the biofilm matrix, as a hydrogel, could respond physically to environmental changes, and hence alter biofilm mechanics, for example by swelling or deswelling in response to external osmotic pressure. Recently, we and others showed that the concentration of agar on which biofilms are grown controls biofilm growth primarily by dictating the osmotic pressure of the agar substrate.[13b,30] Indeed, the biofilm matrix will either take up or lose water depending on the osmotic contrast between the biofilm and the agar, potentially altering biofilm mechanics. Consistent with this reasoning, we demonstrate here a strong dependence of the biofilm modulus on the concentration of agar in the substrate (Figure 2b, Figure S3 and Table S1, Supporting Information). Specifically, Figure 2b shows that the rheological properties of the quadruple mutant biofilm (white) are significantly affected by the agar concentration: the value of G'_p declines appreciably with decreasing agar concentration (i.e., with higher osmotic contrast across the biofilm-agar interface,[13b,30] see Figure S4 in the Supporting Information). This trend holds for the $\Delta rbmA\Delta bap1\Delta rbmC$ mutant (red) that possesses an unstructured, easily swollen VPS network lacking proteins that make crosslinks. Introducing RbmA-mediated cell–cell linkages (the $\Delta bap1\Delta rbmC$ strain, green) raises the overall G'_p for all agar concentrations but does not mitigate the decrease in G'_p that occurs upon swelling. By contrast, crosslinking the VPS network with RbmC/Bap1 eliminates the strong dependence of G'_p on agar concentration as shown by the $\Delta rbmA$ biofilm (blue). Nonetheless, the overall G'_p remains low (≈400–700 Pa), suggesting that cell–cell connections are more effective in raising the biofilm modulus than are VPS crosslinks. Again, the WT biofilm, containing the entire complement of matrix components (gray), displays properties of both strengthened networks: the overall G'_p value remains high (≈1 kPa) for all agar concentrations, and thus, is nearly independent of how the agar affects the osmotic pressure contrast. Such a doubly strengthened network structure is reminiscent qualitatively of recently developed tough synthetic gels.[7b,31] From an evolutionary perspective, a robust mechanical response to the environment could be beneficial to *V. cholerae*, which transitions from sea water to fresh water to the human intestine.[12] The possibility exists that other physicochemical changes occur in the substrate (such as changes in stiffness or friction) as the agar concentration is changed that could also contribute to changes in biofilm mechanics.

Our above analyses of biofilm bulk material characteristics reveal that the biofilm has hydrogel-like properties. This finding suggested to us a rationale that could underlie some of the difficulties encountered in thorough biofilm removal via mechanical perturbation. Specifically, hydrogels have low cohesiveness,[31] and hence they easily break into pieces upon mechanical perturbation. That understanding inspired us to imagine alternative strategies for biofilm removal that would enable biofilms to be detached, intact, from substrates. However, to achieve such interfacial fracture requires information about biofilm interfacial properties, and such data are generally lacking. To overcome this issue, we systematically characterized interfacial energies of *V. cholerae* biofilms with respect to air, liquids, and solid substrates.

We first characterized the surface energy γ_f of a biofilm in air using the Owens-Wendt method (**Figure 3**a; Table S2, Supplementary Methods in the Supporting Information).[32] Surprisingly, despite a high water content, the surface of the WT biofilm is highly nonpolar ($\gamma_f^d \approx 30$ mJ m^{-2}) with a negligible polar component ($\gamma_f^p \approx 0$). We confirmed the magnitude of the nonpolar energy using the Zisman method,[33] which measures the contact angles of nonpolar fluids of different surface tensions on a surface, in this case the biofilm surface (Figure 3b). The quantified values are comparable between the two methods ($\gamma_f^d \approx 37$ mJ m^{-2} for the Zisman method), and independent of the substrate agar concentration. Removal of Bap1 makes the biofilm surface become predominantly polar ($\gamma_f^p \approx 54$ mJ m^{-2}), identical to that of the surface of the $\Delta vpsL$ mutant. Indeed, an earlier report noted that *V. cholerae* biofilms are hydrophobic but become hydrophilic upon deletion of the *bap1* gene.[34] Additional deletion of *rbmC* in the $\Delta bap1$ strain further increases the polar nature of the biofilm surface ($\gamma_f^p \approx 60$ mJ m^{-2}). A vivid demonstration of biofilm polarity is shown in Figure 3c and Figure S5 (Supporting Information), in which a WT biofilm and a $\Delta bap1rbmC$ biofilm show differences in affinity for polar (water) and nonpolar (CH$_2$I$_2$) liquids. Hence, Bap1, and to a minor extent, RbmC, behave similarly to surfactant molecules that alter the surface energy of a material. Using the classic Young equation, the interfacial energy between a WT biofilm and water γ_{fw} was determined to be ≈50–60 mJ m^{-2} (Figure 3d). γ_{fw} depends minimally on the agar concentration (Figure 3d), suggesting that interfacial energies are not influenced by the growth conditions of the biofilm. Finally, we note that deleting *rbmA* did not alter these measured values implying that cell–cell connections do not contribute to biofilm surface properties.

As alluded to above, being able to completely remove biofilms has been a challenging goal in medicine and industry. Knowing the hydrophobic nature of *V. cholerae* biofilms, coupled with the above description of their hydrogel-like bulk properties, put us in a position to exploit a simple technique, previously developed by our group, to peel thin hydrophobic films off of hydrophilic substrates using capillary forces.[35] When the carrier substrate of a thin hydrophobic film is slowly dipped into water, the air-water contact line, pinned at the edge of the film on the substrate, initiates a crack and leads to the peeling of the film, provided that penetration of water into the crack is energetically favorable. Applying this technique to a WT *V. cholerae* biofilm allowed us to peel the biofilm off the agar substrate (**Figure 4**a; Figure S6, Video S1, Supporting Information). Moreover, during the peeling process, a constant peeling angle θ_p developed at the triple contact point between the biofilm, the agar substrate, and the water (Figure 4b). An energy balance leads to $\Gamma = \gamma_{fw}(1 - \cos\theta_p)$, in which Γ is the minimum effective mechanical energy (per unit area) required to separate the biofilm from the substrate if no other dissipation mechanism exists.[35,36] Here, we minimized the energy dissipation through viscous effects by performing the peeling at very low speeds.[35] Therefore, capillary peeling, beyond removing the biofilm, provides a way to determine Γ by measuring θ_p. We determined θ_p experimentally for each agar concentration, and we found a small positive correlation (Figure 4c). This method yields Γ values on the order of 4–7 mJ m^{-2} that depend only modestly on agar concentration (Figure 4d).
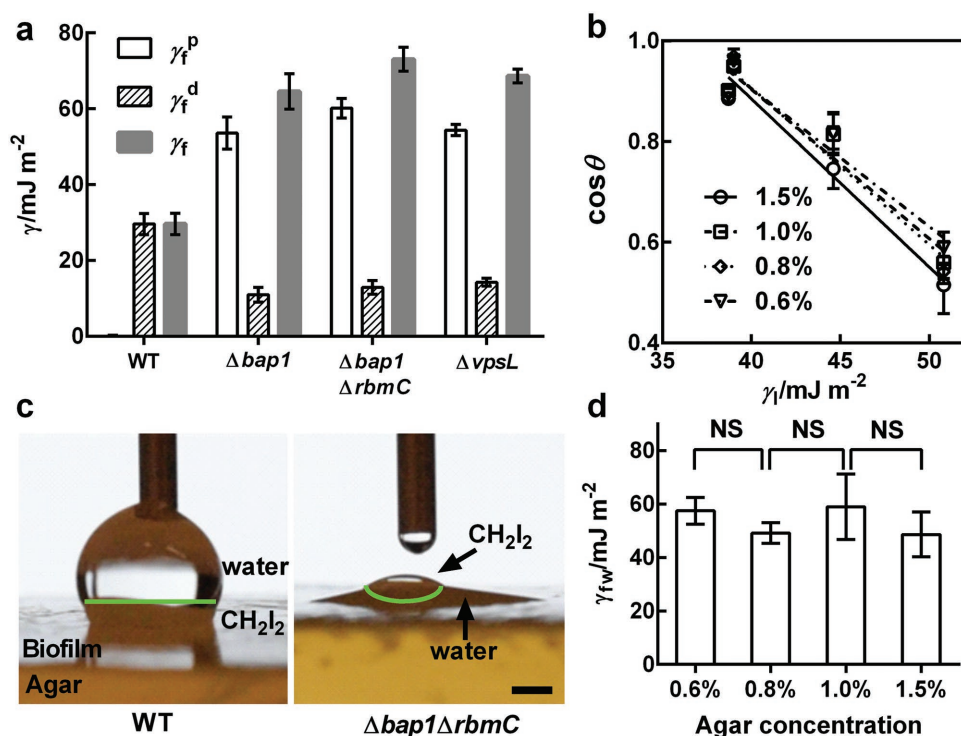
Figure 3. Characterization of biofilm surface energies. a) Measured values of the polar (γ_f^p) and dispersion (γ_f^d) components of the surface energy (γ_f) for the designated *V. cholerae* biofilms grown for two days on 1.5% agar using the Owens–Wendt method.[39] b) Measurement of the surface energies of WT biofilms grown on medium containing the designated concentrations of agar, using the Zisman method.[40] The contact angles θ for nonpolar liquids (CH$_2$I$_2$, CH$_2$Br$_2$, 1-methylnaphthalene, and 1-bromonaphthalene) on biofilms were measured and plotted against the surface energies of the liquids (γ_l) for different concentrations of agar. Linear extrapolation to $\cos\theta = 1$ gives the critical surface tension for wetting γ_c corresponding to the nonpolar component of the surface energy. The symbols designate measurements made for biofilms grown on LB medium solidified with the designated agar concentrations. c) Representative images showing preferential wetting of the WT biofilm by a polar (water) liquid and the $\Delta bap1\Delta rbmC$ mutant biofilm by a nonpolar (CH$_2$I$_2$) liquid, when both liquids were present on top of each biofilm. The green lines denote the interfaces between water and CH$_2$I$_2$. Scale bar: 1 mm. d) Measured biofilm–water interfacial energies γ_{fw} for biofilms grown on medium solidified with the designated concentrations of agar. Unpaired *t*-tests with Welch's correction were performed for statistical analyses. NS stands for not significant. The error bars correspond to standard deviations with $n = 3$.

To demonstrate the thoroughness of biofilm removal using capillary peeling, we imaged live and dead cells in the biofilm before and after peeling (Figure S7, Supporting Information). Most of the live cells were removed from the agar substrate, while some dead cells remained, primarily at the location that harbored the original central core of the biofilm where significant cell death occurs during biofilm growth.[13b,37] Therefore, we suggest that the capillary peeling process could fulfill an unmet need for biofilm removal because it causes interfacial fracture at the biofilm-substrate interface rather than cohesive fracture within the biofilm. To establish optimum conditions for capillary peeling, we scanned different peeling velocities V_{peel} and found that the success rate of peeling decreases with increasing V_{peel} above a threshold value around 0.1 mm s^{-1} (Figure 4e). This observation confirms the quasi-equilibrium nature of the capillary peeling process. If V_{peel} is too high, water passes over the edge of the biofilm and traps the system in a high-energy configuration.

This simple capillary peeling technique can be applied to other biofilm-forming bacterial species and other surfaces. As a proof of concept, we successfully peeled *Pseudomonas aeruginosa* biofilms from agar substrates (Figure S8, Supporting Information). Moreover, we used the capillary peeling procedure to remove biofilms grown on a variety of surfaces, ranging from paper, to semipermeable membranes, to metal (Figure S9, Supporting Information).

Due to the gentle nature of the capillary peeling process, the peeled biofilm remains intact and floats on the liquid used for peeling (Figure 4a, Video S1, Supporting Information). Therefore, in situations in which biofilms need to be grown on one surface and transferred to another, the capillary peeling method provides a convenient option. Indeed, using a substrate with a lower surface energy (untreated glass in this case), the floating biofilm can be picked up without changing its morphology apart from modest swelling (Figure 4f).

We provide two examples to demonstrate the utility of the biofilm transfer technique. First, we imaged the internal structure of a living, peeled biofilm grown at an air-solid interface with single-cell resolution (**Figure 5**a,b), a useful but heretofore inaccessible operation in biofilm research. Moreover, by reversing the dipping direction of the receiving glass substrate, that is by picking up the floating biofilm from each side, we can image the top and bottom of the biofilm, respectively (Figure 5a,b). The bottom layer possesses patches of cells with low fluorescence intensities. In the top layer, by contrast, cells possess strong fluorescence and pack densely. The contrast
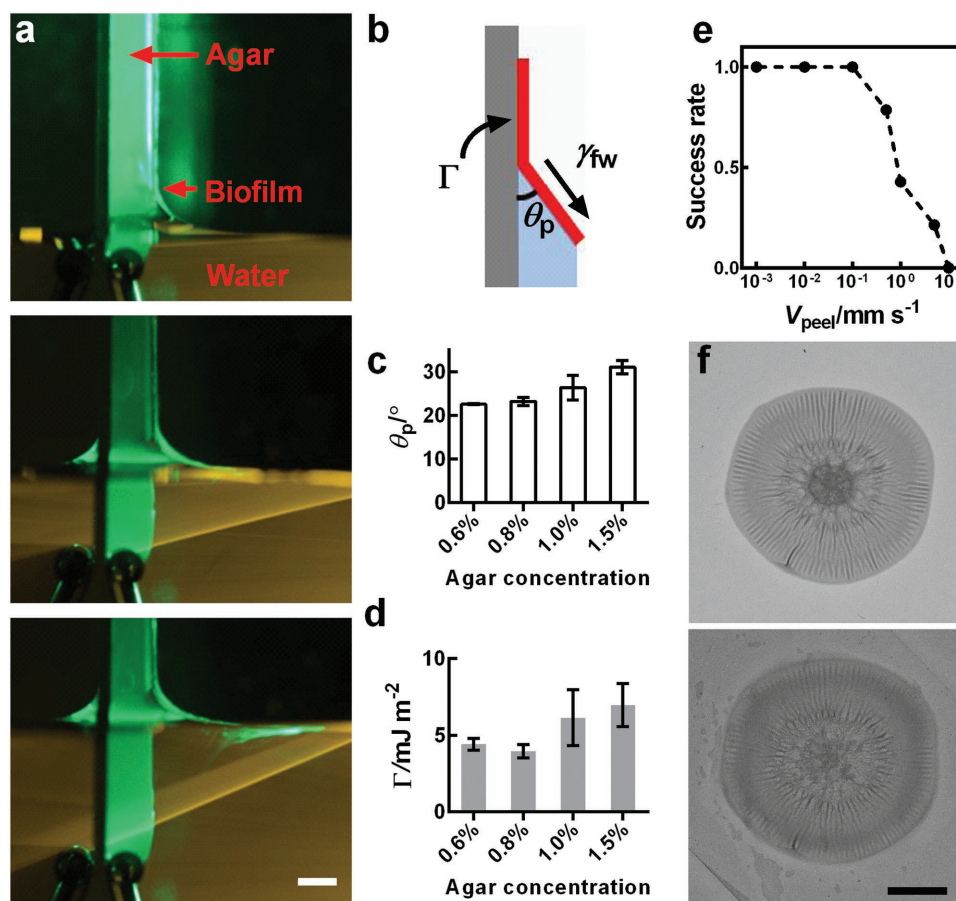
ADVANCED
SCIENCE NEWS
www.advancedsciencenews.com

ADVANCED
MATERIALS
www.advmat.de

Figure 4. Measurement of the adhesion energy between a biofilm and a substrate (agar) using capillary peeling. a) Representative time-lapse images of the capillary peeling process. A green laser sheet illuminates the biofilm and the dye in the water. As the water level rises at a speed of 0.035 mm s^{-1}, the biofilm is peeled off the agar substrate (agar = 0.6%). Scale bar: 3 mm. b) Schematic of the capillary peeling process. The interfacial tension γ_{fw} between the water and the biofilm causes peeling of the biofilm from the substrate, with a constant peeling angle θ_p. Γ denotes the adhesion energy (energy area^{-1}) between the biofilm and the agar substrate. c,d) Peeling angle θ_p and Γ, respectively, as a function of agar concentration. e) Successful peeling as a function of peeling velocity (V_{peel}). Fourteen biofilms were tested at each peeling velocity. The success rate is defined as the ratio between the number of completely removed biofilms and the total number of biofilms. f) Biofilm morphology before (upper) and after (lower) capillary peeling and transfer. Scale bar: 5 mm.

in the internal structures of the top and bottom of the biofilm likely reflects the oxygen gradient present in the original biofilm.[38]

As a second example of the applicability of the capillary peeling method, we peeled biofilms off of agar substrates and floated them on liquid medium containing 50 µg mL^{-1} tetracycline, an antibiotic used to treat clinical *V. cholerae* infections.[39] We compared survival of the floating biofilm cells after 1 h of antibiotic treatment to that of isogenic cells that were grown planktonically to exponential or stationary phase (Figure 5c). Cells in the floating biofilm were significantly more resistant to antibiotic treatment (percent survival $S_{biofilm} \approx 80\%$) than planktonically grown cells ($S_{exponential\ phase} = 6\%$, $S_{stationary\ phase} = 21\%$). To understand whether the increased antibiotic tolerance is due to a biofilm-specific physiological state or due to the spatial structure of the biofilm, we disrupted the floating biofilm immediately prior to antibiotic treatment and repeated the assay (Figure S10, Supporting Information). This treatment caused $S_{biofilm}$ to decrease over threefold (to 24%) to nearly the level of the stationary phase planktonic cells. This result indicates that

the biofilm spatial structure, rather than some biofilm-specific cellular state,[40] is responsible for increased tolerance to antibiotics. Indeed, the effectiveness of antibiotic treatment tracked with the amount of surface area the biofilm had in contact with the antibiotic-containing medium: if the floated biofilm was submerged in the antibiotic-containing medium so that tetracycline could diffuse in from both sides of the biofilm, $S_{biofilm}$ declines to an intermediate level (≈57%). Consistent with this observation, using live–dead staining, we observed that cells in the biofilm interior showed higher survival than cells close to the antibiotic-containing medium (Figure S10, Supporting Information). Future experiments including visualization of the distribution of antibiotic molecules throughout the biofilm could reveal the underlying mechanism of the increased antibiotic resistance of biofilm cells.[41]

Currently the capillary peeling method is limited to biofilms that have been grown statically at an air-solid interface, which provides the necessary means for an external liquid to come into contact with the biofilms and initiate the peeling process. Going forward, we envision two potential strategies to remove
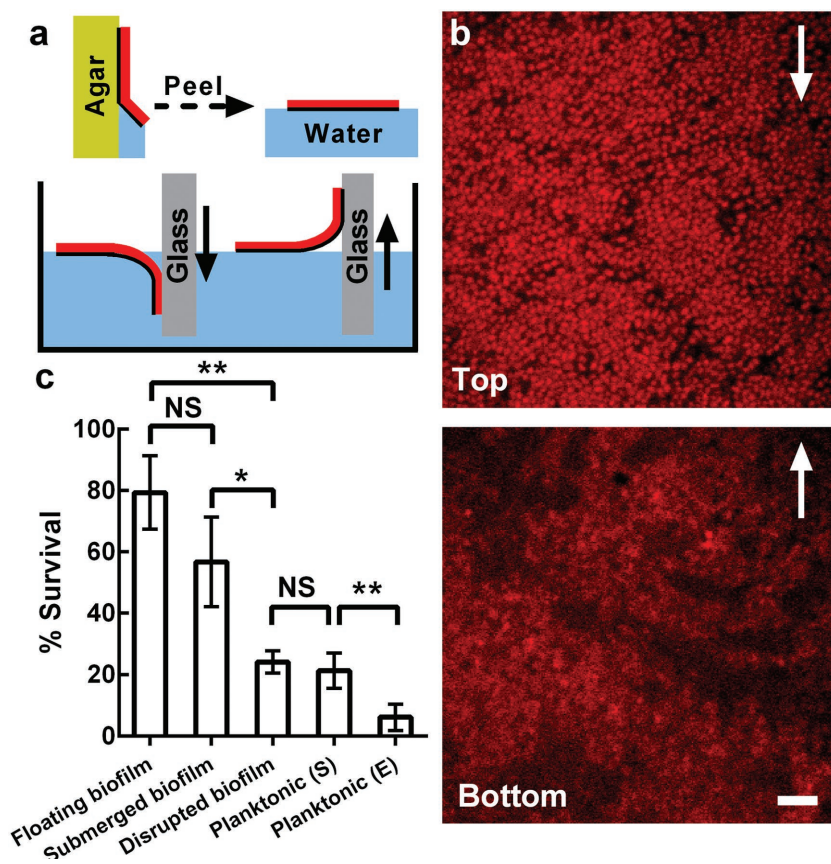
Figure 5. Application of the biofilm transfer technique. a) Schematic of biofilm transfer procedures. Yellow denotes agar. Red denotes the biofilm. Blue denotes water. Gray denotes the glass receiving surface. The black lines highlight the bottoms of the biofilms. The solid arrows indicate the direction of motion of the glass, which is the receiving surface. b) High-resolution imaging of the top (upper) and bottom (lower) of the WT *V. cholerae* biofilm architecture imaged through the glass coverslips used for pick-up. Cells constitutively express *mKate2* from the chromosome. The arrows indicate the direction of the corresponding glass motion during the picking-up step in (a). Scale bar: 5 μm. c) Percentage survival of cells grown planktonically, either to stationary phase (S) or to exponential phase (E), or of cells grown in biofilms, peeled off the surface, and subsequently subjected to 1 h treatment with 50 μg mL^{-1} tetracycline in three different configurations: floated, submerged, or submerged as disrupted pieces. NS stands for not significant; * denotes $P < 0.05$, ** denotes $P < 0.01$, *** denotes $P < 0.001$. The error bars correspond to standard deviations with $n = 4$. An agar concentration of 0.6% was used for all experiments in this figure.

biofilms grown under liquids. First, if submerged biofilms could be dried out, the same capillary peeling method should apply. Second, the capillary peeling method hints at the general possibility of exploiting interfacial energies to remove biofilms from surfaces. Hence, we expect that introducing air bubbles into the medium could potentially generate similar triple contact points and thus remove biofilms that have been grown under liquid.[42]

We envision a variety of applications for the capillary peeling technique. For example, in biofilm infections in wounds, applying appropriate fluids to slowly detach the infectious biofilm could possibly be used instead of the common practice of mechanical debridement.[5c] This technique could also facilitate basic research investigations. For example, it is difficult to study biofilm-host interactions in vitro due to problems encountered in growing host cells and biofilms together under laboratory conditions.[43] The capillary peeling technique could enable scientists to grow the bacterial and host cells separately and bring them into contact at the time of choosing. Also in terms of fundamental biofilm studies, the capillary peeling process yields a convenient measurement of the adhesion energy Γ between a biofilm and a substrate. An alternative method for measurement of bulk biofilm adhesion energy is a micromanipulation method that involves scraping biofilms off substrates and integrating the forces measured during scraping.[11,44] However, such measurements are confounded by the significant energy dissipation caused by friction and deformation, rather than detachment of the biofilm. Therefore, such measures suffer from overestimation of the adhesion energy. Indeed, our measured Γ value of ≈4–7 mJ m^{-2} is an order of magnitude lower than values reported with the scraping method. We argue that we are measuring the actual, close-to-equilibrium work of adhesion between a biofilm and a substrate.

To conclude, we used *V. cholerae* as a model biofilm former to systematically reveal connections between bulk rheological and interfacial biofilm properties, the biocomponents that make up the biofilm material, and relevant external conditions. We discovered *V. cholerae* biofilms to be soft, hydrophobic materials possessing a dual-network internal structure with surface polarity that can be tuned by altering the matrix composition. The discovery of a dual-network structure might allow biofilms to be used as materials for bioengineering, as the strength and chemistry of both the cellular and the polymer networks can be independently manipulated. The understanding gained here also points to new design approaches to disrupt or enhance biofilms by targeting specific components in the biofilm matrix. Finally, we demonstrated capillary peeling as a simple method to measure the adhesion energy and to remove and/or transfer intact biofilms, steps which are otherwise difficult. The capillary peeling technique can be integrated into current or future treatments of biofilm-related infections and industrial processes.

Experimental Section

Strains and Media: All *V. cholerae* strains used in this study were derivatives of the wild-type *Vibrio cholerae* O1 biovar El Tor strain C6706, harboring a missense mutation in the *vpvC* gene (VpvC W240R).[13a] This mutation causes *V. cholerae* cells to have elevated c-di-GMP level and to constitutively produce biofilms. Additional mutations were engineered into this strain using *Escherichia coli* S17 *λpir* carrying pKAS32. All *P. aeruginosa* strains used in this study were derivatives of the wild-type PA14 strain. Mutants were constructed using established procedures.[45]

A strain list is provided in Table S3 (Supporting Information). All strains were grown in lysogeny both (LB) medium at 37 °C with shaking. When designated, fresh LB medium solidified with different percentages of agar was used. To measure the osmotic pressure of agar substrates, dextran solutions were prepared by adding dextran powder (1500-2800 kDa, Sigma-Aldrich) to LB medium followed by shaking at 30 °C overnight.

Microscopy: Transmission images were taken with a home-built setup consisting of an LED illumination pad (Huion) and a Nikon D3300 camera equipped with a macrolens (Sigma). Fluorescence images were obtained using a Leica stereoscope with GFP and mCherry filter sets or with no filter (reflection mode). High-resolution confocal images were acquired with a Yokogawa CSU-X1 confocal spinning disk unit mounted on a Nikon Ti-E inverted microscope, using a 60 × water objective with a numerical aperture of 1.2 plus a 1.5 × post-magnification lens and an Andor iXon 897 EMCCD camera. A 591 nm laser (OEM DPSS) was used to excite cells expressing *mKate2* as well as to visualize dead cells stained with propidium iodide (BacLight Bacterial Viability Kit, ThermoFisher). A 488 nm laser was used to excite live cells stained with Syto9 (BacLight Bacterial Viability Kit, ThermoFisher).

Biofilm Growth on Agar Plates: *V. cholerae* strains were streaked on LB plates containing 1.5% agar and grown at 37 °C overnight. Individual colonies were inoculated into 3 mL of LB liquid medium containing glass beads, and the cultures were grown with shaking at 37 °C to mid-exponential phase (5–6 h). Subsequently, the cells in the cultures were mixed by vortex, OD_{600} was measured, and the cultures were back diluted to an OD_{600} of 0.5. 1 µL of this inoculum was spotted onto prewarmed agar plates (100 mm) solidified with different percentages of agar. For contact angle measurements, 50 µL of this inoculum was applied to an agar plate and spread with glass beads to enable growth of a biofilm covering the entire plate. Plates were incubated at 37 °C for two days. For capillary peeling experiments, two to four colonies were grown per plate. For rheological measurements, seven colonies were grown per plate for agar concentrations of 0.8% or lower, and sixteen colonies were grown per plate for agar concentrations of 1.0% or 1.5%. Fifteen plates were prepared for each rheological measurement. For *P. aeruginosa* biofilms, 2 µL of overnight cultures of WT *P. aeruginosa* PA14 and mutant strains were spotted onto 60 × 15 mm Petri plates containing 10 mL of 1% TB medium fortified with 40 mg L^{-1} Congo red and 20 mg L^{-1} Coomassie brilliant blue dyes and solidified with 1% agar. *P. aeruginosa* biofilms were grown at 25 °C and images were acquired after 120 h.

Biofilm Growth on Nonagar Substrates: In the case of biofilms grown on paper or on stainlesss steel, two pieces of 3 × 3 cm paper (Whatman) or sheets of 304 stainless steel mesh (McMaster, # 500 × 500) were presterilized with ethanol and placed on top of an agar plate (0.6%). 1 µL of inoculant prepared according to the method described above was spotted onto the paper/stainless steel mesh, and the plate was incubated at 37 °C overnight. In the case of biofilms grown on a semipermeable membrane, the inoculant was spotted onto EMD Millipore, VSWP04700 semipermeable membranes that had been placed on top of the agar, and the plate was incubated at 37 °C for 2 days.

Rheology: All rheological measurements were performed with a stress-controlled Anton Paar Physica MCR 301 rheometer at 37 °C. For each measurement, 100–240 colonies were collected with a pipette tip or a razor blade and transferred onto the lower plate of the rheometer. After sandwiching the biofilms between the upper and lower plates with a gap size of 0.5 mm, silicone oil (5 cSt at 25 °C, Sigma-Aldrich) was applied to surround the biofilm to avoid evaporation. It was confirmed that the silicone oil did not affect the measurement result. Sandblasted surfaces were used for both the upper and lower plates to avoid slippage at the boundary. Oscillatory shear tests were performed. During amplitude sweeps, a strain range of 0.01–2000% was scanned at a fixed frequency of 6.28 rad s^{-1}. During frequency sweeps, a range of 0.1–200 rad s^{-1} was scanned at a fixed strain of 1% (in the linear viscoelastic regime). Segmented linear fittings were applied to $G'(\varepsilon)$ curves on a log-log scale. The strain value at which the two linear lines intersect is defined as ε_Y. G' varied minimally in the plateau region. The fitted G' value at $\varepsilon = 1\%$ was

used as G'_p.[14] Yield stress σ_Y is defined as the stress measured at ε_Y. Three biological replicates were performed for each bacterial strain under each osmotic condition.

Contact Angle and Surface Energy Measurements: Side views of biofilm-liquid interfaces were recorded with a Nikon camera (D3300) equipped with a macrolens (Sigma). For all nonpolar liquids, the static sessile drop method was used, in which a 1 µL droplet was gently deposited onto the biofilm and subsequently imaged. For water, to overcome uptake of water by the underlying biofilm/agar, a dynamic sessile drop method was used. Water was slowly added to the surface by a syringe pump, and the advancing contact angle was measured to approximate the equilibrium contact angle. The contact angle θ was extracted using the Droplet_Analysis plugin in ImageJ. Two methods were used to calculate the biofilm-air surface energy γ_f. In the Owens-Wendt method,[32] the contact angles of water and CH_2I_2 on biofilms were measured and, by knowing the dispersion (nonpolar) and polar components of the surface energies of the liquids, two linear equations can be written to solve for the polar γ_f^p and dispersion γ_f^d portions of the total biofilm surface energy γ_f. In the Zisman method,[33] the contact angles θ of four different nonpolar liquids (CH_2I_2, CH_2Br_2, 1-methylnaphthalene, and 1-bromonaphthalene, all from Sigma-Aldrich) on the biofilm were measured. Plotting their surface tensions γ_l versus $\cos\theta$ (Figure 3b) resulted in a straight line. Linear extrapolation to $\cos\theta = 1$ yielded the critical surface tension of wetting γ_c as an approximation for γ_f^d. Once γ_f was determined, γ_{fw} was calculated using the Young equation $\gamma_f - \gamma_{fw} = \gamma_w \cos\theta$.

Peeling Angle Measurements: A piece of agar (≈2 cm × 2 cm) on which a biofilm was grown for two days was transferred onto a 1 inch × 3 inch glass, and secured with a clamp. The setup was attached vertically to a stationary stand. Underneath the biofilm, a water bath containing Rhodamine B was placed on a translational stage (Thorlabs) and moved upward with a controlled velocity to initiate peeling. A cylindrical lens (Thorlabs) was mounted on a 543 nm laser (BioRay) to generate a laser sheet that illuminated the biofilm from the side. The peeling process was recorded with a Nikon camera at a 90° angle. Peeling angles were measured manually using the Nikon Element software at five time points and averaged. Three biological replicates were performed for each condition.

Biofilm Removal and Transfer: For biofilms grown directly on agar plates, the entire agar plate was slowly dipped into water. For biofilms grown on other surfaces, each piece of paper/membrane/stainless steel mesh was individually dipped into water. The biofilm was peeled off of the substrate and floated at the water-air interface. Subsequently, an untreated coverslip was dipped into water to pick up the floated biofilm. Before and immediately after transfer, the biofilm and the original substrate were imaged with a Leica Stereoscope or with a Nikon camera. SytoX green nucleic acid stain (ThermoFisher) was added to the agar at 5 µg mL^{-1} to label dead cells. Live cells constitutively express *mKate2*.

Antibiotic Killing Assay: The killing assay was adapted and modified from refs. [19,41a]. First, pieces of agar (≈2 cm × 2 cm) on which biofilms were grown for two days were transferred onto a 1 inch × 3 inch glass. These setups were vertically dipped into 50 mL Corning conical tubes containing 25 mL of liquid LB medium and glass beads. The biofilms were gently peeled off of the agar substrates and floated at the air-liquid interfaces. The LB medium either contained or lacked 50 µg mL^{-1} of tetracycline. The conical tubes were left at 37° for 1 h, and subsequently, vigorously mixed by vortex for 1 min. 1 mL of the suspensions were transferred to Eppendorf tubes containing small glass beads (acid-washed, 425–500 µm, Sigma), mixed by vortex for 1 min, and serially diluted onto LB plates. The LB plates were incubated overnight at 37° and, subsequently, assessed for colony forming units (CFU). The ratios between CFUs with and without tetracycline treatment were defined as the percent survival. The identical procedure was used for experiments with submerged biofilms except that, immediately after the biofilm was peeled off of the agar substrate, the biofilm was gently pushed completely into the antibiotic-containing medium. For experiments using disrupted biofilms, the conical tube containing the peeled biofilm was agitated by vigorous vortex for 1 min prior to

antibiotic treatment. In experiments involving planktonic cells, the cells were grown to mid-exponential (5 h) or stationary (12 h) phase in liquid LB medium at 37°. Subsequently, the cultures were diluted 100-fold into LB medium with or without tetracycline. The final culture densities were adjusted to make it so that planktonically grown and biofilm-grown cell densities were comparable.

Supporting Information

Supporting Information is available from the Wiley Online Library or from the author.

Conflict of Interest

The authors declare no conflict of interest.

[1] M. Ghannoum, M. Parsek, M. Whiteley, P. Mukherjee, *Microbial Biofilms*, ASM Press, Washington, DC **2015**.

[2] a) R. Nerenberg, *Curr. Opin. Biotechnol.* **2016**, *38*, 131; b) A. E. Franks, N. Malvankar, K. P. Nevin, *Biofuels* **2010**, *1*, 589.

[3] G. M. Marco, *J. Phys. D: Appl. Phys.* **2016**, *49*, 203001.

[4] L. Hobley, C. Harkins, C. E. Macphee, N. R. Stanley-Wall, *FEMS Microbiol. Rev.* **2015**, *39*, 649.

[5] a) H.-C. Flemming, J. Wingender, *Nat. Rev. Microbiol.* **2010**, *8*, 623; b) B. W. Peterson, Y. He, Y. Ren, A. Zerdoum, M. R. Libera, P. K. Sharma, A.-J. van Winkelhoff, D. Neut, P. Stoodley, H. C. van der Mei, H. J. Busscher, *FEMS Microbiol. Rev.* **2015**, *39*, 234; c) D. G. Vernita, D.-F. Megan, K. Kristin, A. R. Christopher, *J. Phys. D: Appl. Phys.* **2017**, *50*, 223002; d) J. N. Wilking, T. E. Angelini, A. Seminara, M. P. Brenner, D. A. Weitz, *MRS Bull.* **2011**, *36*, 385.

[6] A. Dragoš, Á. T. Kovács, *Trends Microbiol.* **2017**, *25*, 257.

[7] a) N. Billings, A. Birjiniuk, T. S. Samad, P. S. Doyle, K. Ribbeck, *Rep. Prog. Phys.* **2015**, *78*, 036601; b) C. Even, C. Marlière, J.-M. Ghigo, J.-M. Allain, A. Marcellan, E. Raspaud, *Adv. Colloid Interface Sci.* **2017**, *247*, 573; c) L. Pavlovsky, J. G. Younger, M. J. Solomon, *Soft Matter* **2013**, *9*, 122; d) O. Lieleg, M. Caldara, R. Baumgartel, K. Ribbeck, *Soft Matter* **2011**, *7*, 3307.

[8] I. Klapper, C. J. Rupp, R. Cargo, B. Purvedorj, P. Stoodley, *Biotechnol. Bioeng.* **2002**, *80*, 289.

[9] a) A. Y. Chen, Z. Deng, A. N. Billings, U. O. S. Seker, M. Y. Lu, R. J. Citorik, B. Zakeri, T. K. Lu, *Nat. Mater.* **2014**, *13*, 515; b) X. Jin, I. H. Riedel-Kruse, *Proc. Natl. Acad. Sci. USA* **2018**, *115*, 3698.

[10] A. K. Epstein, B. Pokroy, A. Seminara, J. Aizenberg, *Proc. Natl. Acad. Sci. USA* **2011**, *108*, 995.

[11] P. Shivapooja, Q. Wang, B. Orihuela, D. Rittschof, P. López Gabriel, X. Zhao, *Adv. Mater.* **2013**, *25*, 1430.

[12] E. J. Nelson, J. B. Harris, J. G. J. Morris, S. B. Calderwood, A. Camilli, *Nat. Rev. Microbiol.* **2009**, *7*, 693.

[13] a) S. Beyhan, F. H. Yildiz, *Mol. Microbiol.* **2007**, *63*, 995; b) J. Yan, C. D. Nadell, H. A. Stone, N. S. Wingreen, B. L. Bassler, *Nat. Commun.* **2017**, *8*, 327.

[14] K. Kovach, M. Davis-Fields, Y. Irie, K. Jain, S. Doorwar, K. Vuong, N. Dhamani, K. Mohanty, A. Touhami, V. D. Gordon, *npj Biofilms Microbiomes* **2017**, *3*, 1.

[15] M. Rubinstein, R. H. Colby, *Polymer Physics*, Oxford University Press, New York **2003**.

[16] M. Wloka, H. Rehage, H. C. Flemming, J. Wingender, *Colloid Polym. Sci.* **2004**, *282*, 1067.

[17] J. K. Teschler, D. Zamorano-Sanchez, A. S. Utada, C. J. A. Warner, G. C. L. Wong, R. G. Linington, F. H. Yildiz, *Nat. Rev. Microbiol.* **2015**, *13*, 255.

[18] F. Yildiz, J. Fong, I. Sadovskaya, T. Grard, E. Vinogradov, *PLoS One* **2014**, *9*, e86751.

[19] F. H. Yildiz, G. K. Schoolnik, *Proc. Natl. Acad. Sci. USA* **1999**, *96*, 4028.

[20] J. C. N. Fong, A. Rogers, A. K. Michael, N. C. Parsley, W.-C. Cornell, Y.-C. Lin, P. K. Singh, R. Hartmann, K. Drescher, E. Vinogradov, L. E. P. Dietrich, C. L. Partch, F. H. Yildiz, *eLife* **2017**, *6*, e26163.

[21] a) V. Berk, J. C. N. Fong, G. T. Dempsey, O. N. Develioglu, X. W. Zhuang, J. Liphardt, F. H. Yildiz, S. Chu, *Science* **2012**, *337*, 236; b) J. C. N. Fong, F. H. Yildiz, *J. Bacteriol.* **2007**, *189*, 2319; c) C. Absalon, K. Van Dellen, P. I. Watnick, *PLoS Pathog.* **2011**, *7*, e1002210.

[22] a) K. Drescher, C. D. Nadell, H. A. Stone, N. S. Wingreen, B. L. Bassler, *Curr. Biol.* **2014**, *24*, 50; b) F. Azam, F. Malfatti, *Nat. Rev. Microbiol.* **2007**, *5*, 782.

[23] a) W. F. Reichert, D. Göritz, E. J. Duschl, *Polymer* **1993**, *34*, 1216; b) G. P. Baeza, C. Dessi, S. Costanzo, D. Zhao, S. Gong, A. Alegria, R. H. Colby, M. Rubinstein, D. Vlassopoulos, S. K. Kumar, *Nat. Commun.* **2016**, *7*, 11368; c) G. Filippone, M. Salzano de Luna, *Macromolecules* **2012**, *45*, 8853.

[24] H. Wang, J. J. Wilksch, T. Lithgow, R. A. Strugnell, M. L. Gee, *Soft Matter* **2013**, *9*, 7560.

[25] P. J. Lu, E. Zaccarelli, F. Ciulla, A. B. Schofield, F. Sciortino, D. A. Weitz, *Nature* **2008**, *453*, 499.

[26] M. Ganesan, S. Knier, J. G. Younger, M. J. Solomon, *Macromolecules* **2016**, *49*, 8313.

[27] J. Yan, A. G. Sharo, H. A. Stone, N. S. Wingreen, B. L. Bassler, *Proc. Natl. Acad. Sci. USA* **2016**, *113*, E5337.

[28] a) K. M. Giglio, J. C. Fong, F. H. Yildiz, H. Sondermann, *J. Bacteriol.* **2013**, *195*, 3277; b) M. Maestre-Reyna, W.-J. Wu, A. H. J. Wang, *PLoS One* **2013**, *8*, e82458.

[29] a) I. W. Sutherland, *Trends Microbiol.* **2001**, *9*, 222; b) M. Tallawi, M. Opitz, O. Lieleg, *Biomater. Sci.* **2017**, *5*, 887; c) S. C. Chew, B. Kundukad, T. Seviour, J. R. C. van der Maarel, L. Yang, S. A. Rice, P. Doyle, S. Kjelleberg, *mBio* **2014**, *5*, e01536.

[30] A. Seminara, T. E. Angelini, J. N. Wilking, H. Vlamakis, S. Ebrahim, R. Kolter, D. A. Weitz, M. P. Brenner, *Proc. Natl. Acad. Sci. USA* **2012**, *109*, 1116.

[31] a) J. P. Gong, Y. Katsuyama, T. Kurokawa, Y. Osada, *Adv. Mater.* **2003**, *15*, 1155; b) J.-Y. Sun, X. Zhao, W. R. K. Illeperuma, O. Chaudhuri, K. H. Oh, D. J. Mooney, J. J. Vlassak, Z. Suo, *Nature* **2012**, *489*, 133.

[32] D. K. Owens, R. C. Wendt, *J. Appl. Polym. Sci.* **1969**, *13*, 1741.

**ADVANCED
SCIENCE NEWS**

www.advancedsciencenews.com

**ADVANCED
MATERIALS**

www.advmat.de

[33] a) D. S. Weisberg, M. Dworkin, *Appl. Environ. Microbiol.* **1983**, *45*, 1338; b) W. A. Zisman, in *Contact Angle, Wettability, and Adhesion*, Vol. *43* (Ed: F. M. Fowkes), Americal Chemical Society, Los Angeles, CA, USA **1964**, p. 1.

[34] E. C. Hollenbeck, J. C. N. Fong, J. Y. Lim, F. H. Yildiz, G. G. Fuller, L. Cegelski, *Biophys. J.* **2014**, *107*, 2245.

[35] S. Khodaparast, F. Boulogne, C. Poulard, H. A. Stone, *Phys. Rev. Lett.* **2017**, *119*, 154502.

[36] K. Kendall, *J. Phys. D* **1971**, *4*, 1186.

[37] M. Asally, M. Kittisopikul, P. Rué, Y. Du, Z. Hu, T. Çağatay, A. B. Robinson, H. Lu, J. Garcia-Ojalvo, G. M. Süel, *Proc. Natl. Acad. Sci. USA* **2012**, *109*, 18891.

[38] L. E. P. Dietrich, C. Okegbe, A. Price-Whelan, H. Sakhtah, R. C. Hunter, D. K. Newman, *J. Bacteriol.* **2013**, *195*, 1371.

[39] M. Kitaoka, S. T. Miyata, D. Unterweger, S. Pukatzki, *J. Med. Microbiol.* **2011**, *60*, 397.

[40] J. W. Costerton, P. S. Stewart, E. P. Greenberg, *Science* **1999**, *284*, 1318.

[41] a) G. Stone, P. Wood, L. Dixon, M. Keyhan, A. Matin, *Antimicrob. Agents Chemother.* **2002**, *46*, 2458; b) B. S. Tseng, W. Zhang, J. J. Harrison, T. P. Quach, J. L. Song, J. Penterman, P. K. Singh, D. L. Chopp, A. I. Packman, M. R. Parsek, *Environ. Microbiol.* **2013**, *15*, 2865.

[42] a) S. Khodaparast, M. K. Kim, J. E. Silpe, H. A. Stone, *Environ. Sci. Technol.* **2017**, *51*, 1340; b) W. G. Pitt, M. O. McBride, A. J. Barton, R. D. Sagers, *Biomaterials* **1993**, *14*, 605.

[43] P. S. Stewart, *Pathog. Dis.* **2014**, *70*, 212.

[44] M. J. Chen, Z. Zhang, T. R. Bott, *Biotechnol. Tech.* **1998**, *12*, 875.

[45] a) L. R. Hmelo, B. R. Borlee, H. Almblad, M. E. Love, T. E. Randall, B. S. Tseng, C. Lin, Y. Irie, K. M. Storek, J. J. Yang, R. J. Siehnel, P. L. Howell, P. K. Singh, T. Tolker-Nielsen, M. R. Parsek, H. P. Schweizer, J. J. Harrison, *Nat. Protoc.* **2015**, *10*, 1820; b) S. Mukherjee, A. C. Bree, J. Liu, J. E. Patrick, P. Chien, D. B. Kearns, *Proc. Natl. Acad. Sci. USA* **2015**, *112*, 250.

ADVANCED MATERIALS

Supporting Information

Bacterial Biofilm Material Properties Enable Removal and Transfer by Capillary Peeling

Jing Yan, Alexis Moreau, Sepideh Khodaparast, Antonio Perazzo, Jie Feng, Chenyi Fei, Sheng Mao, Sampriti Mukherjee, Andrej Košmrlj, Ned S. Wingreen, Bonnie L. Bassler,* and Howard A. Stone*

WILEY-VCH

Supporting Information

Bacterial Biofilm Material Properties Enable Removal and Transfer by Capillary Peeling

Jing Yan, Alexis Moreau, Sepideh Khodaparast, Antonio Perazzo, Jie Feng, Chenyi Fei, Sheng Mao, Sampriti Mukherjee, Andrej Košmrlj, Ned S. Wingreen, Bonnie L. Bassler, Howard A. Stone**

Table S1. Summary of measured rheological properties of *V. cholerae* biofilms.

V. cholerae Strain	Agar Conc.[a]	Parameters			Comments
		G'_P/kPa	ε_Y	σ_Y/kPa	
WT	0.6%	1.11 ± 0.16	0.13 ± 0.05	0.10 ± 0.03	With dual networks
	0.8%	1.16 ± 0.30	0.15 ± 0.00	0.12 ± 0.03	
	1.0%	1.12 ± 0.18	0.15 ± 0.07	0.14 ± 0.07	
	1.5%	1.38 ± 0.07	0.17 ± 0.03	0.17 ± 0.03	
Δ*rbmA*	0.6%	0.59 ± 0.12	0.18 ± 0.02	0.08 ± 0.02	With crosslinked polymer network only
	0.8%	0.54 ± 0.10	0.20 ± 0.02	0.09 ± 0.01	
	1.0%	0.42 ± 0.11	0.27 ± 0.04	0.09 ± 0.01	
	1.5%	0.70 ± 0.04	0.27 ± 0.03	0.15 ± 0.01	
Δ*bap1* Δ*rbmC*	0.6%	0.76 ± 0.15	0.10 ± 0.01	0.05 ± 0.02	With cellular network only
	0.8%	1.14 ± 0.05	0.09 ± 0.02	0.08 ± 0.01	
	1.0%	1.30 ± 0.12	0.13 ± 0.01	0.13 ± 0.01	
	1.5%	1.63 ± 0.12	0.18 ± 0.02	0.21 ± 0.02	
Δ*rbmA* Δ*bap1* Δ*rbmC*	0.6%	0.11 ± 0.02	0.38 ± 0.01	0.03 ± 0.00	With non-crosslinked polymer network only
	0.8%	0.20 ± 0.02	0.36 ± 0.01	0.05 ± 0.00	
	1.0%	0.31 ± 0.04	0.35 ± 0.02	0.07 ± 0.00	
	1.5%	0.69 ± 0.05	0.28 ± 0.01	0.14 ± 0.01	
Δ*vpsL*	0.6%	0.23 ± 0.10	0.15 ± 0.02	0.02 ± 0.01	No polymer network, accessory matrix proteins nonfunctional
	0.8%	0.43 ± 0.12	0.13 ± 0.00	0.04 ± 0.01	
	1.0%	0.67 ± 0.10	0.13 ± 0.00	0.06 ± 0.01	
	1.5%	1.13 ± 0.25	0.15 ± 0.02	0.12 ± 0.04	
Δ*rbmA* Δ*vpsL*	0.6%	0.14 ± 0.05	0.12 ± 0.02	0.01 ± 0.00	No polymer network, accessory matrix proteins nonfunctional
	0.8%	0.29 ± 0.01	0.11 ±0.02	0.02 ± 0.00	
	1.0%	0.45 ± 0.08	0.12 ± 0.01	0.03 ± 0.01	
	1.5%	1.04 ± 0.13	0.13 ± 0.00	0.10 ± 0.04	
Δ*rbmA* Δ*bap1* Δ*rbmC* Δ*vpsL*	0.6%	0.12 ± 0.06	0.13 ± 0.05	0.01 ± 0.00	No polymer network, no accessory matrix proteins
	0.8%	0.23 ± 0.06	0.11 ± 0.02	0.02 ± 0.00	
	1.0%	0.36 ± 0.09	0.12 ± 0.02	0.04 ± 0.01	
	1.5%	0.90 ± 0.24	0.14 ± 0.03	0.11 ± 0.01	

a) Abbreviation for agar concentration in the substrate.

Table S2. Summary of measured contact angles for surface energy calculations.

V. cholerae Strain	Agar Conc.[d]	H$_2$O	CH$_2$I$_2$	Liquid 1-Br-NP[e]	1-Me-NP[f]	CH$_2$Br$_2$
WT	0.6%	109 ± 4°	54 ± 2°	35 ± 4°	27 ± 2°	16 ± 2°
WT	0.8%	105 ± 3°	57 ± 1°	35 ± 1°	28 ± 1°	14 ± 3°
WT	1.0%	111 ± 10°	56 ± 3°	35 ± 4°	26 ± 1°	18 ± 2°
WT	1.5%	105 ± 6°	59 ± 4°	42 ± 3°	28 ± 1°	17 ± 3°
Δ*bap1*[a]	1.5%	31 ± 4°	76 ± 4°	N/A	N/A	N/A
Δ*bap1*Δ*rbmC*[b]	1.5%	11 ± 1°	70 ± 4°	N/A	N/A	N/A
Δ*vpsL*[c]	1.5%	21 ± 1°	68 ± 2°	N/A	N/A	N/A

a) Strain lacking a key surface-active matrix protein.

b) Strain lacking two key surface-active matrix proteins.

c) Strain lacking the key matrix polysacharride.

d) Abbreviation for agar concentration in the substrate.

e) Abbreviation for 1-bromonaphthalene.

f) Abbreviation for 1-methylnaphthalene.

Table S3. Bacterial strains and plasmids used in this study.

| Strains/plasmids	Relevant Features	Reference
E. coli		
S17 λ-*pir*	Wild Type	[1]
DH5α	F⁻ *endA1 glnV44 thi-1 recA1 relA1 gyrA96 deoR nupG purB20* φ80d*lacZ*ΔM15 Δ(*lacZYA-argF*) U169, hsdR17($r_K^-m_K^+$), λ⁻	Laboratory stock
SM10λ*pir*	*thi thr leu tonA lacY supE recA*::RP4-2-Tc::Mu	Laboratory stock
V. cholerae		
C6706*str*2	El Tor Wild Type	[2]
JY283	*vpvC*^W240R Δ*pomA* (denoted WT)	[3]
JY284	*vpvC*^W240R Δ*pomA*Δ*rbmA*	[3]
JY285	*vpvC*^W240R Δ*pomA*Δ*bap1*Δ*rbmC*	[3]
JY286	*vpvC*^W240R Δ*pomA*Δ*rbmA*Δ*bap1*Δ*rbmC*	[3]
JY287	*vpvC*^W240R Δ*pomA*Δ*vpsL*	[3]
JY288	*vpvC*^W240R Δ*pomA*Δ*rbmA*Δ*vpsL*	This study
JY290	*vpvC*^W240R Δ*pomA*Δ*rbmA*Δ*bap1*Δ*rbmC*Δ*vpsL*	This study
JY370	*vpvC*^W240R Δ*pomA lacZ*:P_tac-*mKate2*:*lacZ*	[3]
JY393	*vpvC*^W240R Δ*pomA*Δ*rbmC*	[3]
JY400	*vpvC*^W240R Δ*pomA*Δ*bap1*	[3]
P. aeruginosa		
UCBPP-PA14	Wild Type	Laboratory stock
SM404	Δ*pelA*	[4]
SM1141	Δ*P_pelA*::*P_hyspank*-*pelABCDEFG*	This study
Plasmid		
pKAS32	Suicide vector, Amp^R Sm^S	[5]
pNUT144	Suicide vector, Amp^R Kan^R Sm^S	[6]
pNUT157	pNUT144 *vpvC*^W240R	[6]
pCMW112	pKAS32 Δ*vpsL*	[7]
pCN004	pKAS32 *lacZ*:P_tac-*mKate2*:*lacZ*	[8]
pCN007	pKAS32 Δ*rbmA*	[9]
pCN008	pKAS32 Δ*rbmC*	[9]
pCN009	pKAS32 Δ*bap1*	[3]
pCDN010	pKAS32 Δ*pomA*	[9]
pEXG2	Allelic exchange vector with pBR origin, gentamicin resistance, *sacB*	[10]
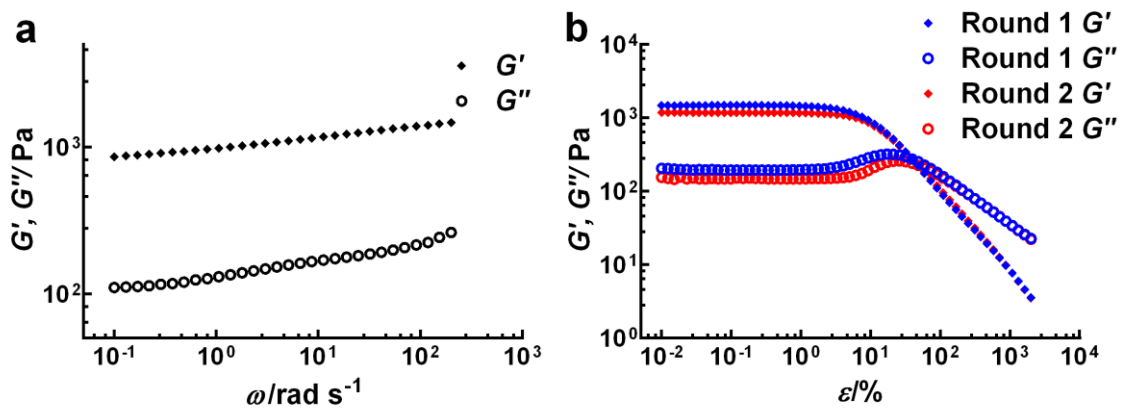
Figure S1. *V. cholerae* biofilms behave as hydrogels. a) Storage modulus *G'* (filled diamonds) and loss modulus *G"* (open circles) of WT *V. cholerae* biofilms grown for two days on plates with 0.6% agar, as a function of frequency ω, measured in a parallel-plate geometry. b) Storage modulus *G'* and loss modulus *G"* of the same *V. cholerae* biofilm samples as a function of the amplitude of oscillatory shear strain ε. The red curves were measured immediately after the blue curves. Irreversible structural changes during yielding cause a modest decrease in both *G'* and *G"* in the second round of measurements.
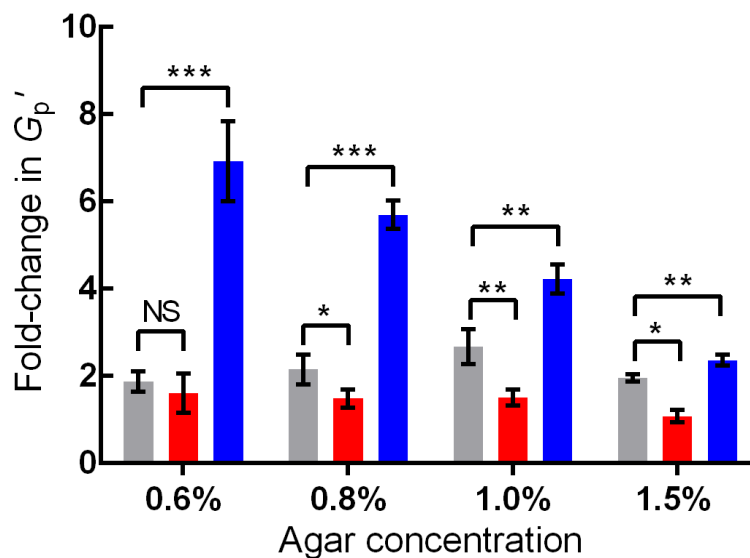
Figure S2. RbmA-mediated cell-cell connections strengthen biofilms in a VPS and RbmC/Bap1-dependent manner. Plotted are fold-changes in G'_p in biofilms made of cells possessing *rbmA* compared to those lacking *rbmA* that are otherwise WT (gray), Δ*vpsL* (red), and Δ*bap1*Δ*rbmC* (blue). The bacterial strains were grown on plates with the designated agar concentrations. NS stands for not significant; * denotes $P < 0.05$, ** denotes $P < 0.01$, *** denotes $P < 0.001$. Error bars correspond to standard deviations with $n = 3$. In the absence of VPS, RbmA cannot mediate cell-cell connections to increase G'_p (i.e. red bars are not significantly different from a value = 1). This result is consistent with previous microscopy results showing that the retention of RbmA in a *V. cholerae* biofilm requires VPS.[11] On the other hand, in the absence of RbmC/Bap1, the strengthening effect of RbmA-mediated cell-cell connections is amplified compared to its strengthening effect in the WT (compare blue to gray bars).
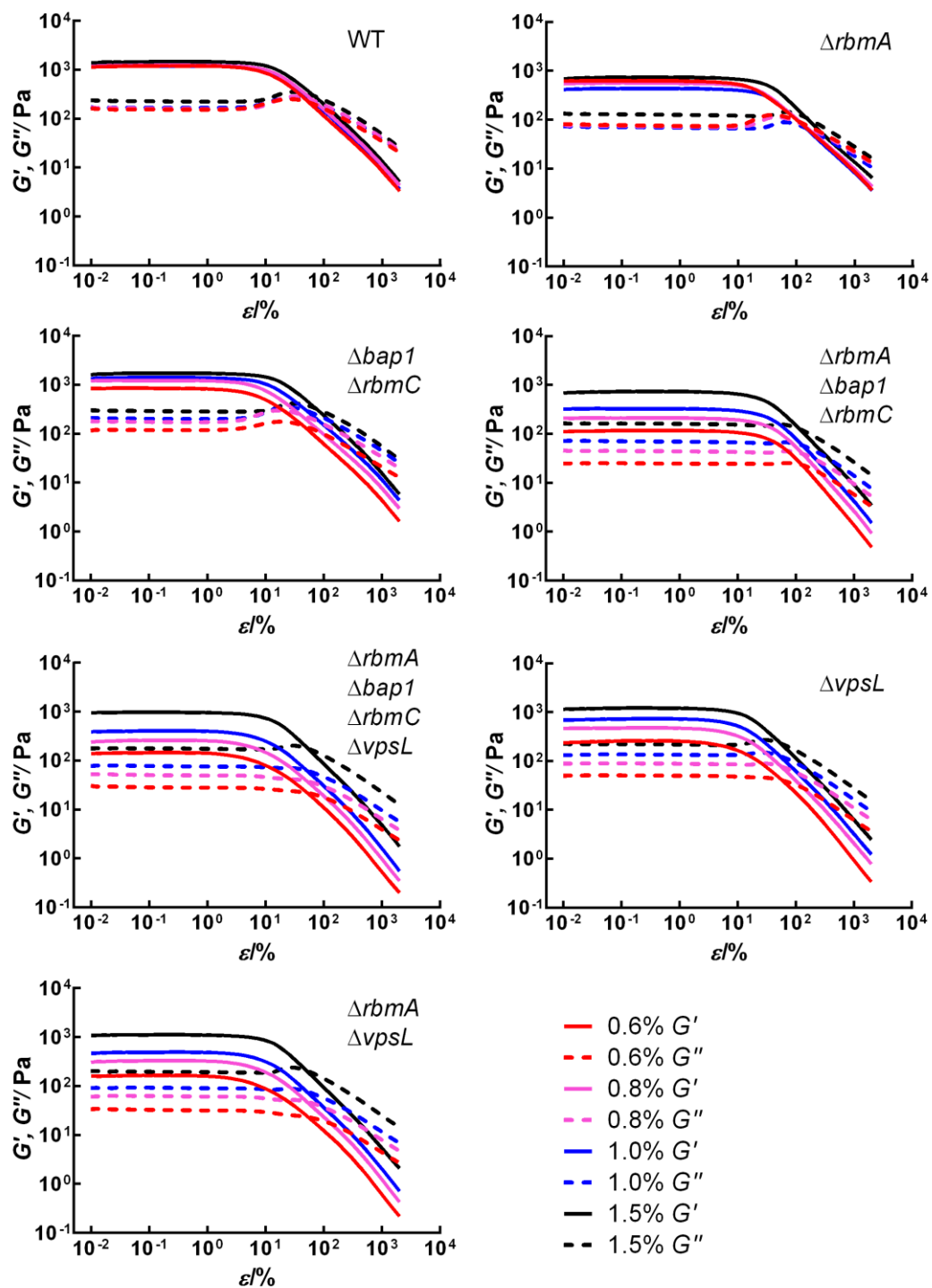
Figure S3. Complete rheological data for main Figures 1-2, Figure S2, and Table S1. Shown are the storage modulus G' (solid curves) and loss modulus G'' (dashed curves) as a function of the amplitude of oscillatory strain ε for the *V. cholerae* strains indicated on the plots.
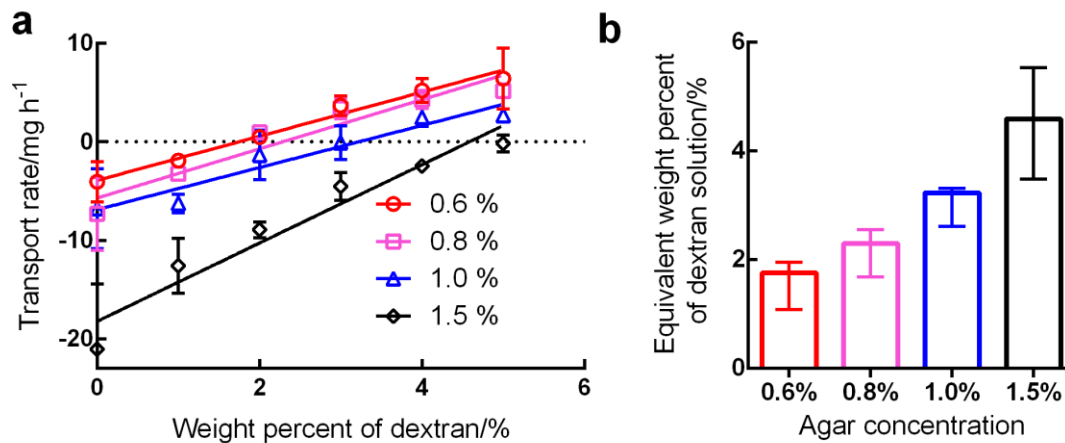
Figure S4. Measurement of osmotic pressures of agar substrates. a) A droplet of LB medium containing dextran was placed on a semi-permeable membrane on top of different concentration agar substrates (0.6-1.5%). Depending on the dextran concentration in the droplet and the agar concentration in the substrate, an osmotic contrast is established across the semi-permeable membrane. Thus, the liquid droplet either takes up water from the agar or loses water to the agar. Using linear interpolation, we identified the concentration of dextran at which there is zero net flow across the membrane. We used these values as proxies for the osmotic pressures of the agar at each concentration, shown in (b). Importantly, we find that the osmotic pressure of agar plates is equivalent to polymer concentrations between 1-5%, which is on the order of the matrix polysaccharide concentration in the biofilm.[3] Specifically, in our earlier contribution, we found that the volume fraction of the vibrio polysaccharide matrix is ~ 1-4% of the extracellular biofilm space.[3] Therefore, depending on the agar concentration, the biofilm matrix will either take up or lose water,[3, 12] similar to the dextran droplet in the above experiments. Error bars correspond to standard deviations in (a) and 95% confidence intervals in (b).
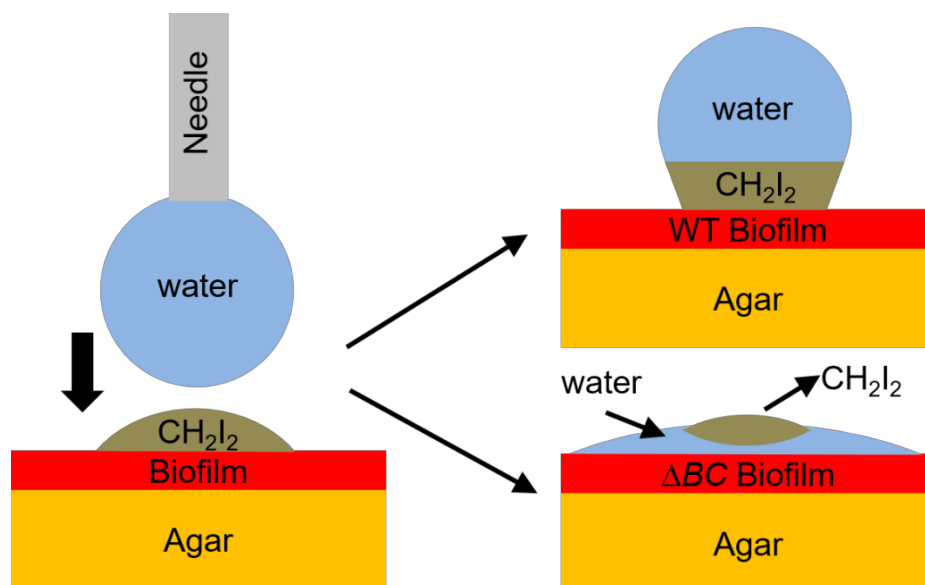
Figure S5. Schematic representation of the experiment in main Figure 3c. Not drawn to scale. Depending on the polarity of the biofilm, either water or CH_2I_2 is in preferential contact with the biofilm.
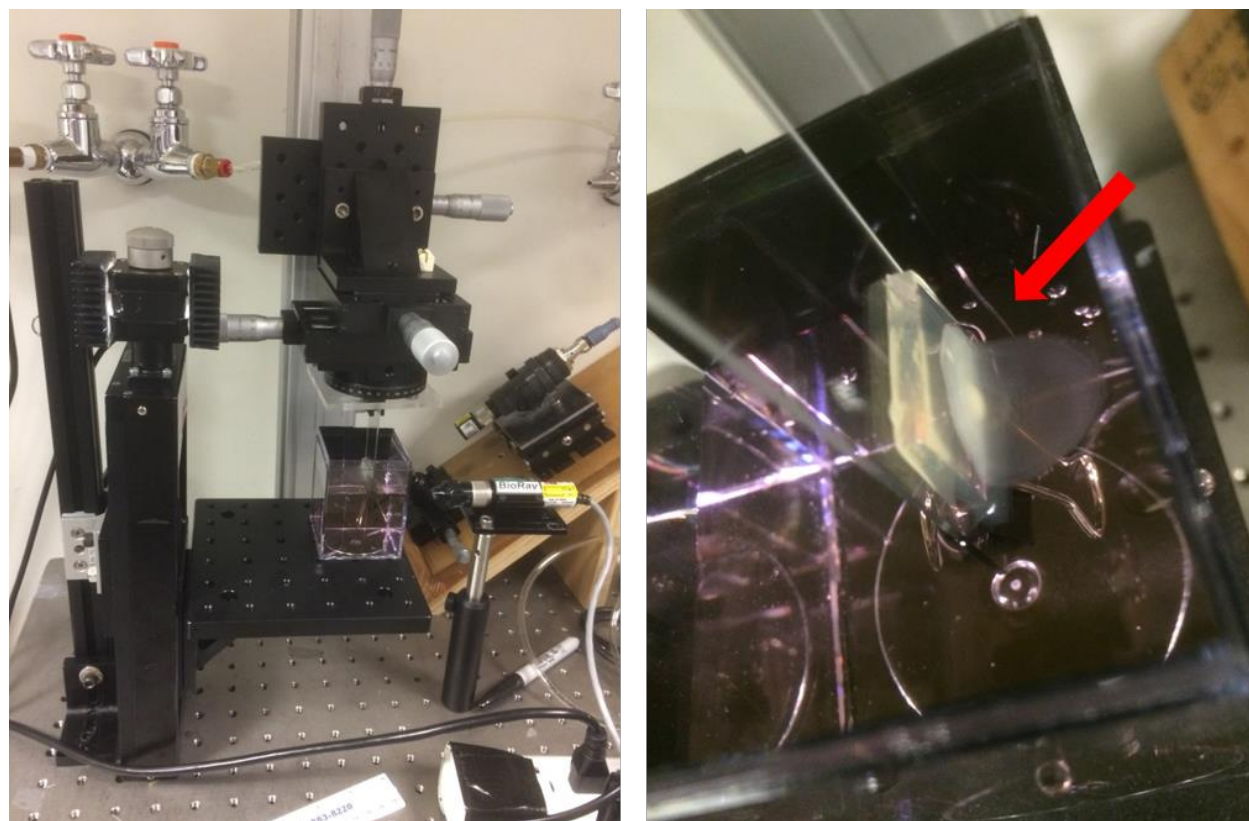
Figure S6. *Left*: Image of the experimental setup for capillary peeling with controlled peeling velocity. *Right*: Close-up view of the biofilm. The red arrow indicates the position of the *V. cholerae* biofilm. Half of the biofilm has been peeled off and floats on the water while the other half remains adhered to the agar substrate.

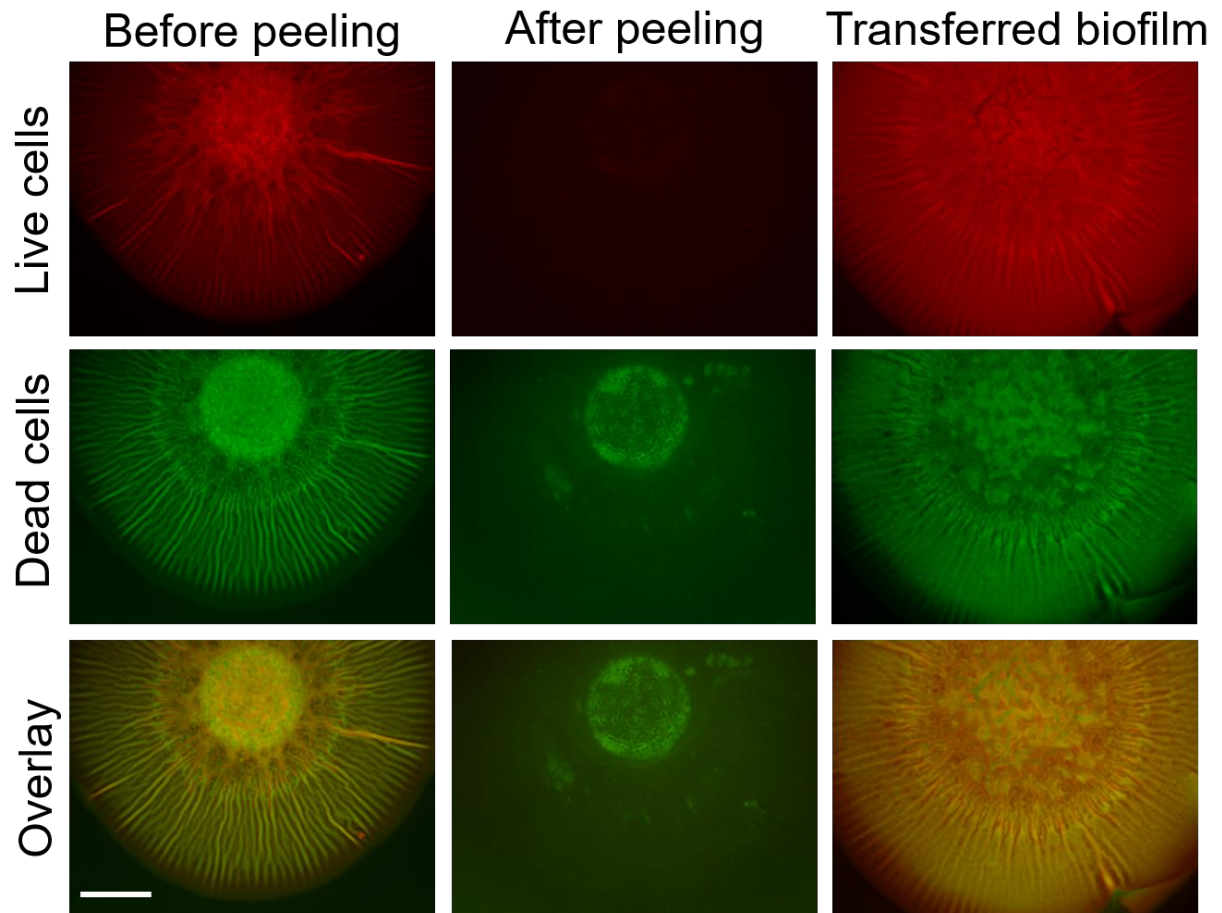|	Before peeling	After peeling	Transferred biofilm
Live cells			
Dead cells			
Overlay			

Figure S7. Capillary peeling as a biofilm removal and transfer technique. Shown are fluorescence images of the agar substrate (0.6%) before (*left*) and after (*middle*) capillary removal of a WT *V. cholerae* biofilm, as well as the images of the transferred biofilm (*right*). Red (*top*) is fluorescence from mKate2 in live cells. Green (*middle*) corresponds to SytoX DNA staining of dead cells. *Bottom* row shows images by overlaying the red and green channels. Scale bar: 3 mm.
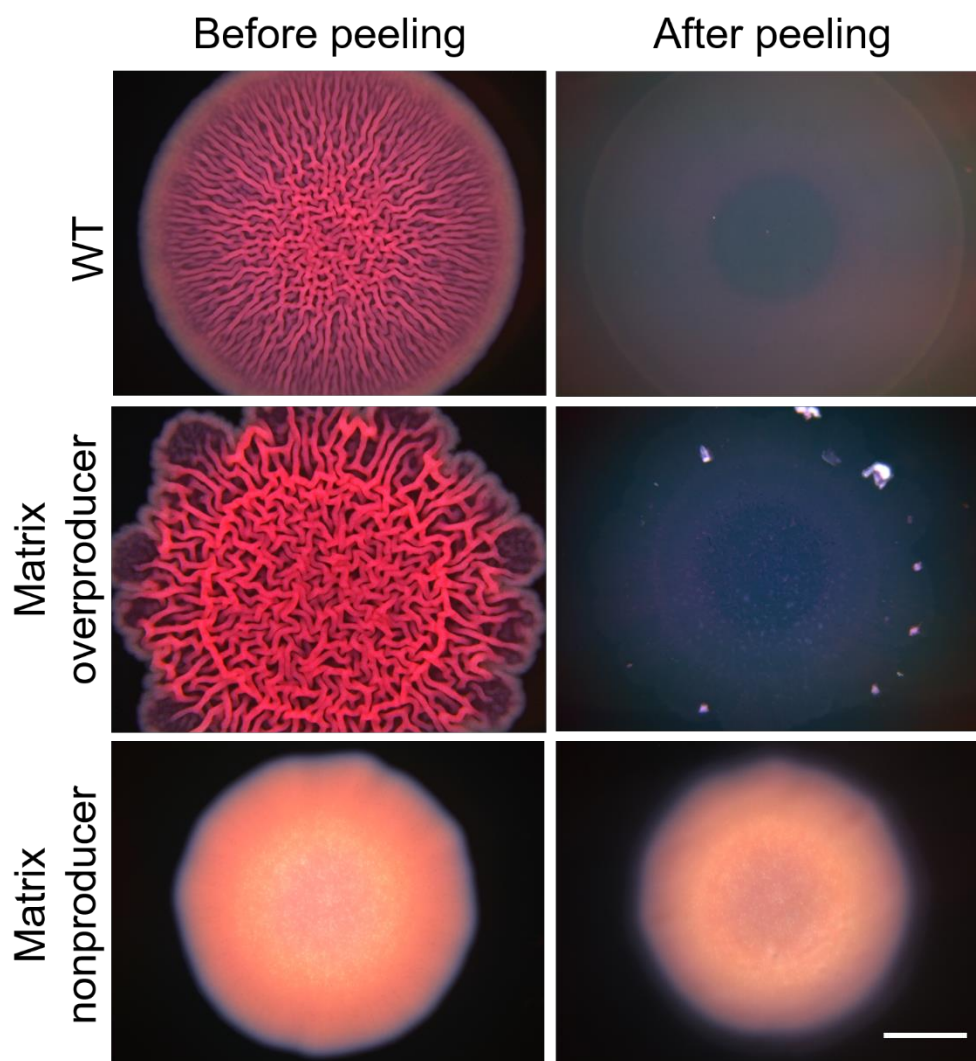
Figure S8. Capillary peeling of *Pseudomonas aeruginosa* biofilms grown on 1.0% agar substrates containing congo red dye. Images of the biofilms taken before peeling are shown on the *left* and images of the agar substrates after peeling are shown on the *right*. From *top* to *bottom* are biofilms of WT *P. aeruginosa* PA14, a *P. aeruginosa* PA14 strain that overproduces the Pel matrix polysaccharide, and a *P. aeruginosa* PA14 strain that lacks Pel (See Table S3 for details). *P. aeruginosa* biofilms can only be peeled off an agar substrate if the strain produces the matrix polysacharide. Scale bar: 3 mm.
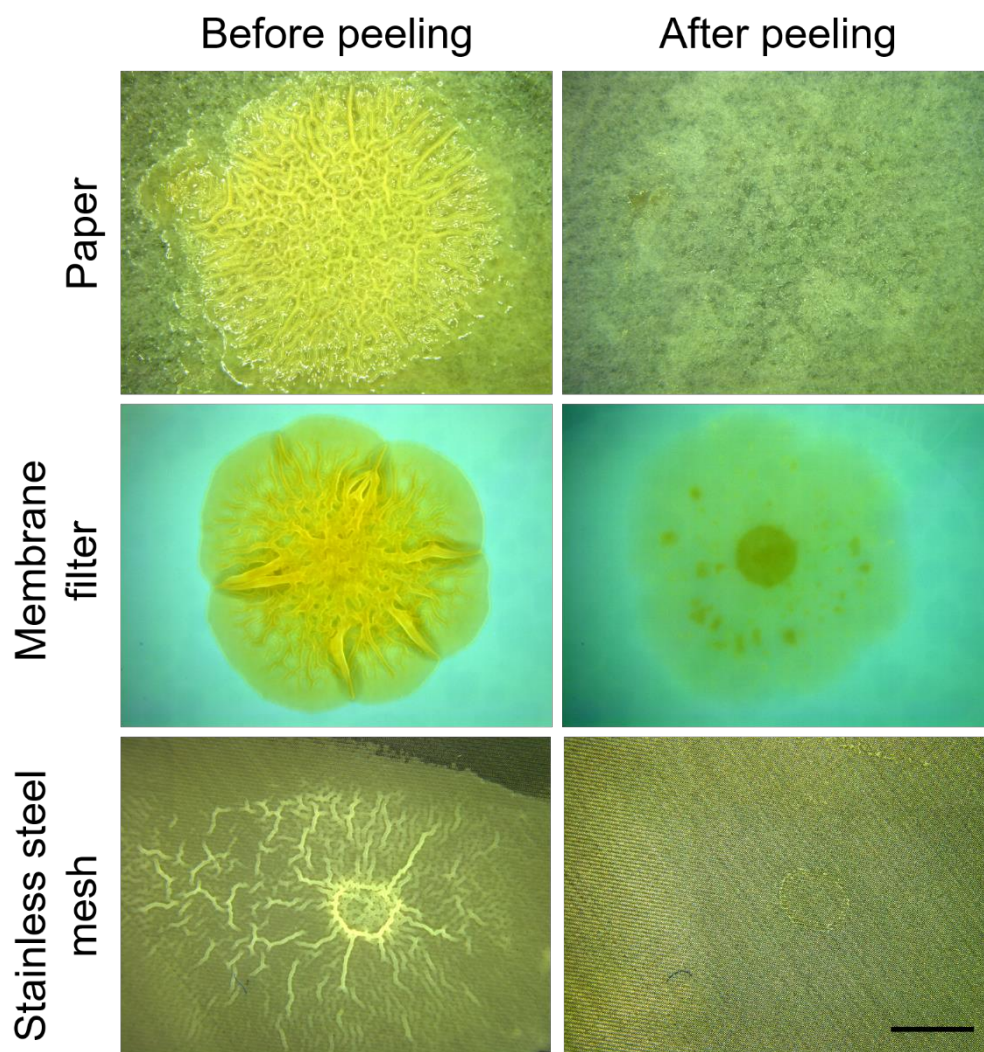
Figure S9. Application of the capillary peeling method to *V. cholerae* biofilms grown on different substrates (See Methods for growth conditions). Biofilm images before peeling are shown on the *left* and surface images after peeling are shown on the *right*. Scale bar: 3 mm.
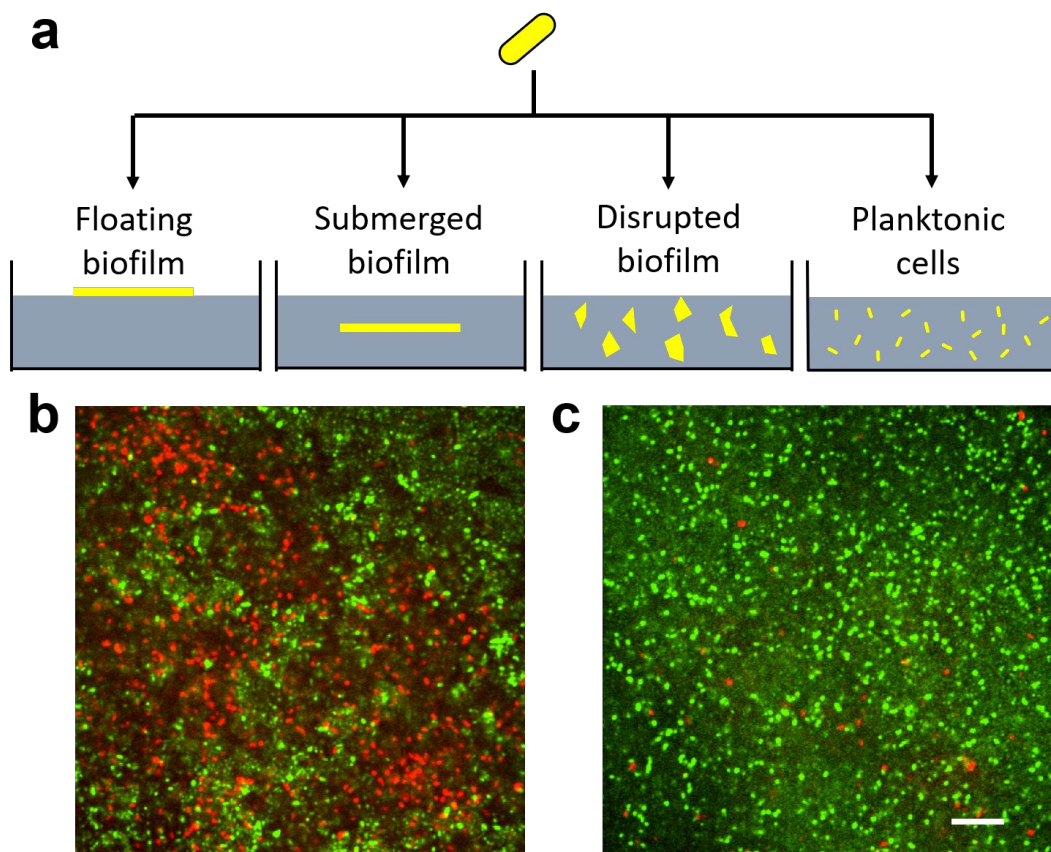
a

b **c**

Figure S10. Application of the biofilm transfer technique. a) Schematic representation of the experiment in main Figure 5c. Yellow denotes *V. cholerae* cells. Blue denotes the liquid LB medium containing the antibiotic (tetracycline at 50 μg mL^{-1}). Not drawn to scale. b,c) Confocal miscroscopy images of live-dead staining of biofilm-dwelling cells. Green and red signals correspond to live cells and dead cells, respectively. For panels b and c, a WT *V. cholerae* biofilm was grown for two days on a plate containing 0.6% agar. Subsequently, the biofilm was peeled off the agar substrate via the capillary peeling method (left-most schematic in panel a), and floated on LB medium containing tetracycline. After 1 h of antibiotic treatment, the floating biofilm was transferred to a #1.5 glass coverslip with the original base of the biofilm attached to the coverslip (via the *right* configuration in main text Figure 5a). The biofilm was imaged from the bottom through the coverslip. Panel b shows the base of the biofilm and panel c shows an image taken 10 μm above the biofilm base. Scale bar: 10 μm.

Supplementary Methods: Principles of surface energy measurements

The calculation of surface energy follows the original manuscript by Owens and Wendt,[13] which is briefly summarized here. The surface energy of a biofilm γ_f can be decomposed into the nonpolar, dispersion force component γ_f^d and the polar component due to hydrogen bonding and/or dipole-dipole forces γ_f^p,

$$\gamma_f = \gamma_f^d + \gamma_f^p \tag{1}$$

The interfacial energy γ_{fl} between a biofilm and a liquid (l) located on top of the biofilm follows:

$$\gamma_{fl} = (\sqrt{\gamma_f^d} - \sqrt{\gamma_l^d})^2 + (\sqrt{\gamma_f^p} - \sqrt{\gamma_l^p})^2 \tag{2}$$

in which γ_l^d and γ_l^p are the dispersion and polar components of the surface energy of the liquid, respectively. Neglecting the vapor pressure effect, the Young equation for a liquid droplet located on top of a biofilm is:

$$\gamma_l \cos\theta = \gamma_f - \gamma_{fl} \tag{3}$$

where θ is the contact angle. Combining equations (2) and (3), one arrives at the expression:

$$1 + \cos\theta = 2\sqrt{\gamma_f^d}(\frac{\sqrt{\gamma_f^d}}{\gamma_l}) + 2\sqrt{\gamma_f^p}(\frac{\sqrt{\gamma_f^p}}{\gamma_l}) \tag{4}$$

Therefore, by measuring the contact angle θ of two liquids with known γ_l^d, γ_l^p, and γ_l, against a biofilm, simultaneous equations are obtained which can be used to solve for γ_f^d and γ_f^p. We chose water and CH_2I_2 as the test liquids and used the surface energy values reported in the original manuscript by Owens and Wendt.[13]

SI Movie Caption

Video S1: Capillary peeling of a WT *V. cholerae* biofilm grown on a 0.6% agar substrate for two days and subsequent pick-up with a glass substrate. The movie is played in real time.

Supplementary Reference

[1]   V. De Lorenzo, K. N. Timmis, *Methods Enzymol.* **1993**, *235*, 386.

[2]   K. H. Thelin, R. K. Taylor, *Infect. Immun.* **1996**, *64*, 2853.

[3]   J. Yan, C. D. Nadell, H. A. Stone, N. S. Wingreen, B. L. Bassler, *Nat. Commun.* **2017**, *8*, 327.

[4]   S. Mukherjee, D. Moustafa, C. D. Smith, J. B. Goldberg, B. L. Bassler, *PLOS Pathog.* **2017**, *13*, e1006504.

[5]   K. Skorupski, R. K. Taylor, *Gene* **1996**, *169*, 47.

[6]   K. Drescher, C. D. Nadell, H. A. Stone, N. S. Wingreen, B. L. Bassler, *Curr. Biol.* **2014**, *24*, 50.

[7]   B. K. Hammer, B. L. Bassler, *Mol. Microbiol.* **2003**, *50*, 101.

[8]   C. D. Nadell, B. L. Bassler, *Proc. Natl. Acad. Sci. USA* **2011**, *108*, 14181.

[9]   C. D. Nadell, K. Drescher, N. S. Wingreen, B. L. Bassler, *ISME J.* **2015**, *9*, 1700.

[10]   L. R. Hmelo, B. R. Borlee, H. Almblad, M. E. Love, T. E. Randall, B. S. Tseng, C. Lin, Y. Irie, K. M. Storek, J. J. Yang, R. J. Siehnel, P. L. Howell, P. K. Singh, T. Tolker-Nielsen, M. R. Parsek, H. P. Schweizer, J. J. Harrison, *Nat. Protoc.* **2015**, *10*, 1820.

[11]   a) V. Berk, J. C. N. Fong, G. T. Dempsey, O. N. Develioglu, X. W. Zhuang, J. Liphardt, F. H. Yildiz, S. Chu, *Science* **2012**, *337*, 236; b) J. Yan, A. G. Sharo, H. A. Stone, N. S. Wingreen, B. L. Bassler, *Proc. Natl. Acad. Sci. USA* **2016**, *113*, E5337.

[12]   A. Seminara, T. E. Angelini, J. N. Wilking, H. Vlamakis, S. Ebrahim, R. Kolter, D. A. Weitz, M. P. Brenner, *Proc. Natl. Acad. Sci. USA* **2012**, *109*, 1116.

[13]   D. K. Owens, R. C. Wendt, *J. Appl. Polym. Sci.* **1969**, *13*, 1741.